PROCEEDINGS

THE FORTY-FOURTH ANNUAL SYMPOSIUM ON THE

ART OF SCIENTIFIC GLASSBLOWING

1999

THE
AMERICAN SCIENTIFIC GLASSBLOWERS SOCIETY

Princeton Marriott
Princeton, NJ

June 22-27, 1999

Proceedings

The Forty-fourth Annual

Symposium

on the

Art of Scientific Glassblowing

Sponsored by
The American Scientific
Glassblowers Society

THE
AMERICAN SCIENTIFIC GLASSBLOWERS SOCIETY
Thomasville, NC

The American Scientific Glassblowers Society
302 Red Bud Lane
Thomasville, NC 27360
Phone: (336) 882-0174
FAX: (336) 882-0172

Library of Congress #58-3756

Officers and Directors
of
The American Scientific Glassblowers Society
1998-1999

Officers

President	David G. Daenzer
President-Elect	Barry W. Lafler
Secretary	Scott Bankroff
Treasurer	Waine Archer
President Emeritus	Karl Walther

Sectional Directors

Michael Palme
Edwin A. Powell
Timothy Drier
Daniel Wilt
Joseph S. Gregar
Doni J. Hatz
Sean G. Adams
A. Ben Seal
Hans Rohner
Gary Farlow
David Smart
Gary S. Coyne
Jack Korfhage

George Sites
Director Emeritus

James Merritt, Executive Secretary

Dawn Hodgkins, National Office Manager

Marylin C. Brown, Ph.D., *Fusion & Proceedings* Editor

Past Presidents

† J. Allen Alexander
* Karl H. Walther
Arthur Dolenga
Alfred H. Walrod
Richard W. Poole
† William E. Barr
† Charles J. Cassidy
† Jonathan Seckman
William A. Gilhooley
M. Howe Smith
Billie E. Pahl
Theodore W. Bolan
Earl R. Nagle
Werner H. Haak
Gordon Good
Robert G. Campbell
† Helmut E. Drechsel
Lawrence W. Ryan, Jr.
† Joseph W. Baum
Andre W. Spaan
Donald E. Lillie
Wilbur C. Mateyka
Jerry A. Cloninger
† David Chandler
† Owen J. Kingsbury, Jr.
Raymond L. Carew
James K. Merritt
Joseph S. Gregar
Joseph Walas, Jr.
A. Ben Seal
Robert J. Ponton
Ian B. Duncanson
Allan B. Brown
Richard C. Smith
Richard P. Gerhart

† Deceased
* President Emeritus

44TH SYMPOSIUM COMMITTEES

General Chair	Mike Souza Princeton University
Co-Chair	Barry Lafler Brookhaven National Lab
Symposium Coordinator	Jerry Cloninger Georgia Institute of Technology
Artistic Chair	Dennis Briening Hercules Research Center
Exhibits Chair	Sally Prasch Prasch Glass
Junior Seminars Chair	Joseph Gregar Argonne National Lab
Regular Member Seminars Chair	Allan Brown University of Connecticut
Seminar Chair	Barry Lafler Brookhaven National Lab
Seminar Coordinator	Joe Walas East Carolina University
Technical Papers Chair	Wayne Martin M&M Glassblowing Co., Inc.
Technical Papers Coordinator	Michelle Archer
Technical Posters Chair	Ed Powell Zeneca Inc.
Technical Workshops Chair	Ottmar Safferling
Tours	Rudy Schlott State University of New York, Stony Brook

CONTENTS

Papers

Other Information

Papers

Applications and Fabrication of a 1000mm Liquid Nitrogen Cooled Carbon Monoxide Laser

by
Timothy L. Henthorne
Department of Chemistry
The Ohio State University
Columbus, Ohio 43210

Abstract. This paper contains a brief history of the development, function and application of a carbon monoxide laser enclosed in a liquid nitrogen dewar. It then moves into an elaborate description of techniques employed to successfully fabricate this device. Since this is written from the perspective of a glassworker having no prior experience in designing or fabricating this apparatus, the reader will have a unique look into how the problems encountered throughout the fabrication process were successfully solved. In summary, alternate methods will be recommended or suggested which may render a more refined finished product in a more productive manner enhancing functional performance without sacrificing structural integrity.

Introduction: The acronym LASER stands for Light Amplification by Stimulated Emission of Radiation. Lasers produce coherent "light" at specific wave lengths. The term "light" is general and covers radiation produced in the infrared, visible, ultraviolet, and recently, the X-ray portions of the electromagnetic spectrum. A laser device has three essential elements: (1) a suitable laser medium, (2) a pumping process that creates a population inversion, and (3) an optical feedback system. The laser medium consists of an appropriate collection of atoms, molecules, and ions in a gas, liquid, or solid form. Solid devices are further grouped into solid-state and semiconductor (diode) lasers. The pumping process creates a population inversion between quantum-mechanical energy levels. These inversions occur between vibrational/rotational or electronic energy levels. Common pumping methods include DC electrical discharge, RG discharge, chemical, and gas dynamic. Optical feedback is almost always needed to provide longer path lengths which yield higher gain. The optical feedback system usually consists of mirrors or polished surfaces. Most optical cavities consist of two mirrors, a total reflector and an output coupler. The total reflector reflects as much light as possible, upwards of 99.7%. The output coupler is a special mirror that transmits some of the light, usually 5-30%, and reflects the rest. The light transmitted out of the laser cavity becomes a useful coherent power source. For an extensive review of the complex physics behind lasers please see Siegman's book [A].

The laser tube discussed in this paper was built for the Nonequilibrium Thermodynamics Laboratories in the Department of Mechanical Engineering at The Ohio State University. Professor J.W. Rich heads this group which specializes in extreme disequilibrium processes in diatomic molecules (N2, O2, CO, and NO). This includes the measurement and theoretical prediction of rate-constants for molecular energy transfer. This group uses liquid nitrogen cooled CO lasers to create optically pumped plasmas to conduct this proof-of-principle research.

CO lasers can be made to lase on several hundred different vibrational-rotational transitions from v = 37 to 36 down to the v = 1 to 0, thus making it a valuable spectroscopic source [B]. Achieving optical power on the v = 1 to 0 is not easy and has taken years of research. To obtain any power on the v = 1 to 0 transition, the gas mixture must be cryogenically cooled. Early water- cooled versions reached about 25 W of power, but the laser transitions went down to only v = 8 to 7. Cooling the gasses and the laser tube in a liquid nitrogen bath provided substantial gains in total power as well as making laser transitions on the lower vibrational energy levels possible. Most of the current research utilizes these lowest vibrational transitions, thus the technical nightmare of efficiently and repeatedly cooling down the laser gases was born. Early designs used a trough to hold the liquid nitrogen. Brass or stainless steel bellows were used to allow for differences in the coefficients of expansion between the gas plasma tube and the stainless steel trough. This design repeatedly had problems with the liquid nitrogen leaking onto the optical table [C]. The trough design also prohibited the visual monitoring of the laser's discharge. This can cause severe problems with ozone formation due to the addition of oxygen to the gas mixture during optimization. Liquid ozone is a potentially explosive substance under the right conditions (rapid heating and electrical failure to the vacuum pump). These reasons pushed researchers to develop the double jacketed laser tube design, see figure 1. The entire tube is made from borosilicate glass tubing. The inner jacket holds the liquid nitrogen and the space between the inner and outer jackets is evacuated to form a liquid nitrogen dewar around the laser tube and the cooling coils. Most of this laser tube development was done at universities in Bonn, Germany [B], and St. Petersburg, Russia [D].

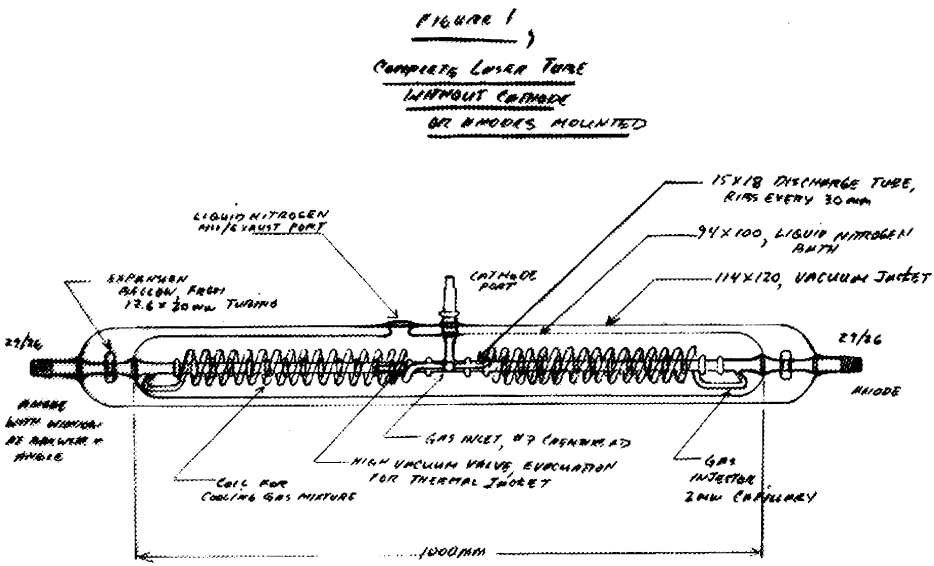

The carbon monoxide plasma tube fabricated at The Ohio State University Glassblowing Facility (figure 1) was a modified version of the type manufactured in Bonn. Modifications included a threaded glass compression fitting serving as a gas inlet to both cooling coils, a single opening serving as a liquid nitrogen fill/exhaust port and the use of a high-vacuum valve through which a dynamic vacuum was applied between the nitrogen

reservoir and the thermal jacket. In addition, the cathode and anodes were redesigned replacing all glass-to-tungsten seals with threaded glass compression fittings to support and seal electrode connections. These changes resulted in a successful, yet simpler version of a 1000-millimeter carbon monoxide laser, which was reported to have performed as efficiently as a 1500-millimeter version previously in use.

A completed carbon monoxide laser tube is composed of several components. Each will be discussed in this paper. These include: the discharge tube with gas cooling coils, the bellows, the liquid nitrogen reservoir, the vacuum jacket, the cathode, and the anodes. Since this device operates under what are perceived to be extreme service conditions (-195.8 degrees Celsius) special attention was given towards selection of materials free of any defects or flaws such as chips, scratches or stones, all of which were believed to have the potential to cause a completed tube to fail (crack).

Fabrication began with the discharge tube assembly (figure 3). Two sections of coil were wound using a stainless steel mandrel coated with graphite (figure 2). The graphite coating helped to assure the finished coil could be easily removed without scratches or other damage. Tubing was spliced together and premeasured. Specifications required a cooling path no less than 182.8 centimeters per coil. Each coil was to be teed off the main gas inlet. To equalize pressure and volume in each coil, the measurement of coil length was thought to be more critical than with previous versions where each coil could be independently adjusted. Upon completion, the coils were annealed and set aside.

FIGURE 2;
COIL DETAILS
RIGHT/LEFT SIDE

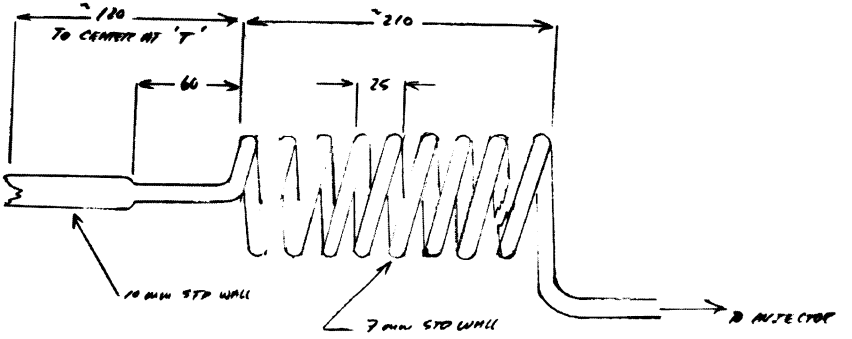

- WIND ON 18" STAINLESS STEEL MANDREL, PITCHED AT 23 mm
- TOTAL LENGTH OF TUBING USED IN COIL, 1828 mm (72")

FIGURE 3, DISCHARGE TUBE DETAILS

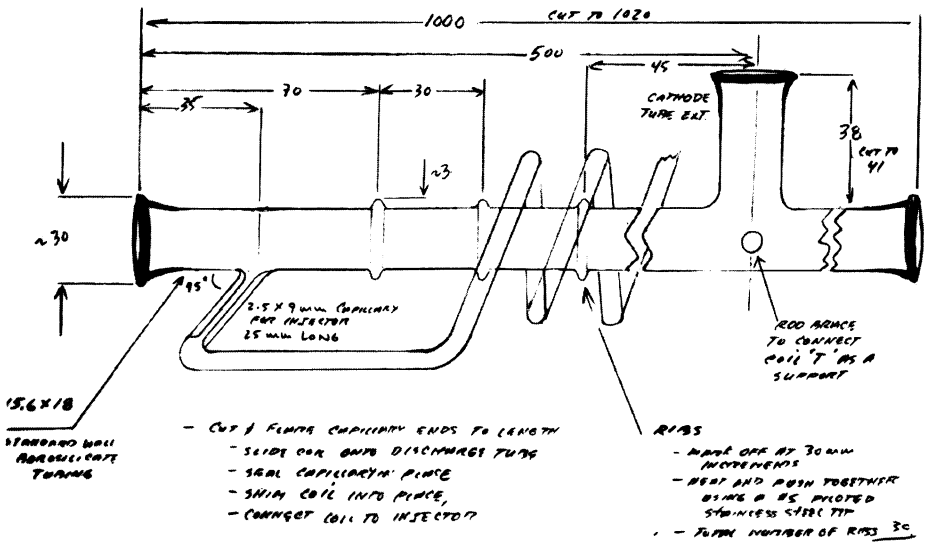

The discharge tube (figure 3) was formed using 15.6 x 18.0-millimeter standard wall borosilicate glass tubing. External ribs were formed every 30-millimeters, on center, over the length of the tube stock. Appropriate room was given at the center of the tube (90 millimeters) for the cathode extension to be teed off and at the ends (70 millimeters) where the injectors were located. This feature served two functions. First, and most important, the ribs served to increase cryogenic cooling of the gas mixture. This radically improved power by nearly fifty percent over a smooth discharge tube [B]. Secondly, it improved the design allowing the tube to contract without failure during cryogenic cooling. Additionally, this feature allowed for expansion and contraction throughout the fabrication process as areas were reheated locally to complete external ring-seals.

With the ribs formed, the ends of the discharge tube were then prepared for sealing through the liquid nitrogen reservoir. The ends of the tube were flared to approximately 30-millimeters in diameter. A heavy lip of glass was formed and the tubing thickness was enhanced throughout the flare. This allowed for robust ring-seals to be formed through the closed ends of the reservoir. Coils were then moved over the ends of the discharge tube on each side of the cathode tee-tub, and positioned in place with shims made of glass fiber tape. The injection nozzles made of 2.5-millimeter inside diameter capillary tubing, were measured, cut to length, flared on each end and then fused into place at 45-degree angles to the wall of the discharge tube. (It was observed that some previously fabricated tubes displayed injectors which were fused into place tangent to the wall of the discharge tube in an effort to create a swirling flow of gas mixture, this detail was not applied.) Straight sections left at the end of each coil were then heated until workable and bent into position where they were fused to the injectors. At the middle, the two coils were joined and teed-off using a sufficient length of 10-millimeter standard wall tubing. A support rod was fused into place opposite the tee-tube and into the wall

of the discharge tube for support. Both the tee-tube for the cathode and the one for the gas injection coils were prepared prior to assembly, having a flared profile with an enhanced sealing lip to help maintain seal integrity through the wall of the liquid nitrogen reservoir.

Specifications for a 1000-millimeter liquid nitrogen cooled laser tube required the discharge tube to vary in straightness no more than 1mm from end to end. (It was later learned this was not a strict specification; the 15.6 millimeter bore of the discharge tube creates a large enough plasma to make up for any slight deviations.) To achieve this, the completed discharge tube assembly was slumped over a pre-straightened quartz mandrel having an outside diameter of 15mm. The lathe-straightened mandrel was tapered on one end allowing it to be inserted into the discharge tube in a vertical position without damage to the inside wall of the tube. (A graphite mandrel was considered for this purpose; time constraints forced the use of quartz.) The mandrel was supported in the oven suspending the assembly from the oven floor by scrap pieces of glass tubing. The entire assembly was leveled. The shims made of glass fiber tape were left in place to support the coil. A satisfactory result was obtained as the oven heated the assembly to 590 degrees Celsius, allowing the glass to "relax" across the mandrel. After the quartz mandrel was removed, a final visual check was performed using a lathe to support each end. Any variance in straightness could be observed through the spindle of the lathe as it turned the part.

FIGURE 4
BELOW

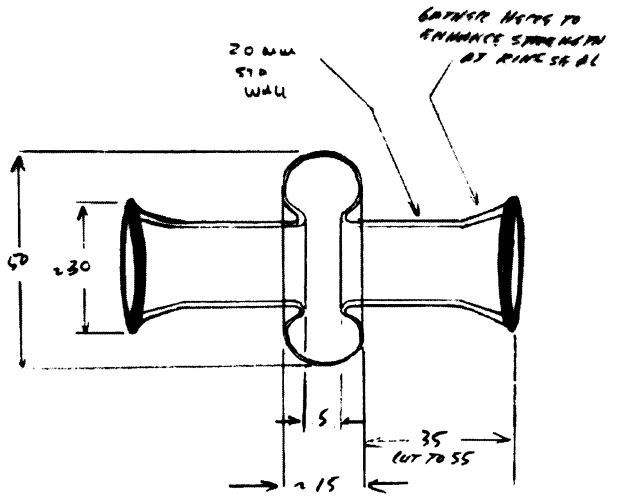

* ALL DIMENSIONS IN mm

* USE 19 MOLY HIGH TIP, STAINLESS

The liquid nitrogen reservoir, complete with the discharge tube assembly was constructed following fabrication of a pair of identical expansion bellows (figure 4). Based on the design of the Bonn tube, bellows sealed between the coolant reservoir and the vacuum jacket served to effectively absorb contraction and expansion of the glass as it responded to normal operating conditions. In addition, the bellows served to support the weight of the filled liquid nitrogen reservoir. Using a large hush tip on a National hand-torch, each bellow was carefully formed in one complete action. A 50-millimeter section of 20-millimeter standard wall tubing was heated in the lathe until it was just above the softening point. At that moment, the glass was forced together by driving the tailstock of the lathe towards the headstock while expelling a breath of air into the tube. A suitable bellow turned in the lathe without an uneven or unbalanced form. The tubing stock was flame cut 15 millimeters longer than the desired finished dimension on each side of the bellow. This additional material allowed for increasing the weight of the glass as the ends of the tube were flared with a heavy sealing lip. (It was observed on existing tubes that this area was commonly susceptible to failure due to inadequate seal weight at the vacuum jacket.) The final pair of expansion bellows was oven annealed and set aside.

A 1200-millimeter section of 94 x 100-millimeter tubing was used to create the liquid nitrogen reservoir. Initial preparation involved basic cleaning of the tube, removing packaging dust and fingerprints. This routine was followed throughout the fabrication process. Specific points were located and marked where the cathode tee-tube extension and the gas injection tee-tube extension were to be ring-sealed through the wall of the reservoir. The areas were gently heated and blown out to form slight bubbles, and were flame annealed. The ends of the tube were slightly flared allowing for easy insertion of the holders, which would temporarily suspend the assembly inside the reservoir tube. The discharge tube assembly was then inserted into the reservoir tube having temporary supports (figure 5) shimmed into each end. Cotton rags were used to prevent scratches as the assembly was carefully moved across the inside of the tube into final position.

FIGURE 5

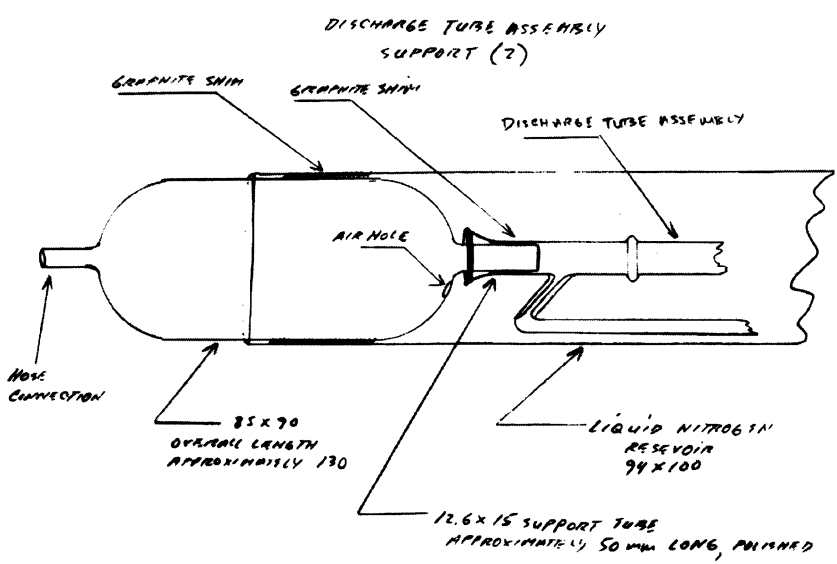

Once in position, each holder was carefully shimmed into place with graphite tape. The tee-tube extensions were positioned up into the previously formed bubbles in the wall of the reservoir. Special care was used to chuck the assembled reservoir in the lathe. Chuck arms were covered with glass tape to prevent any damage to the exterior of the tube.

Work began at the middle section (figures 6 and 7). Each tube extension was sealed into the wall of the reservoir and then reopened to allow for a short extension to be added to the outside of the ring seal. The extensions were adjusted to length in preparation to be ring-sealed through the wall of the vacuum jacket. Once again, the weight of the extensions was enhanced as much as possible. Ring-seals into the wall of the vacuum jacket from these extensions had to endure cryogenic cooling and support the combined weight of the reservoir and coolant.

FIGURE 6

CENTER VIEW, FRONT

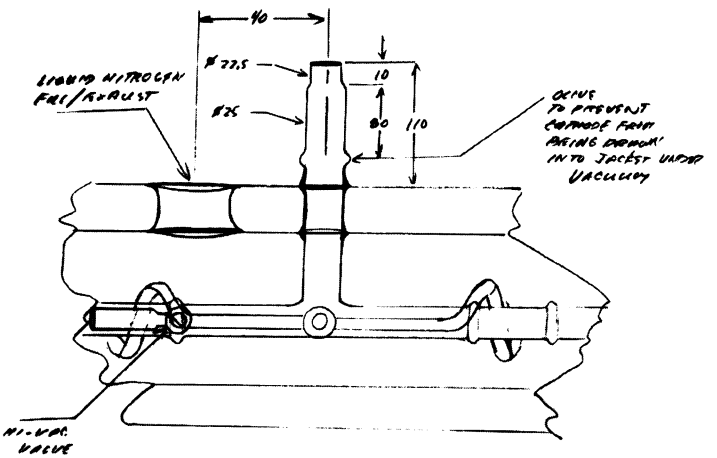

FIGURE 7

TOP VIEW AT MIDDLE

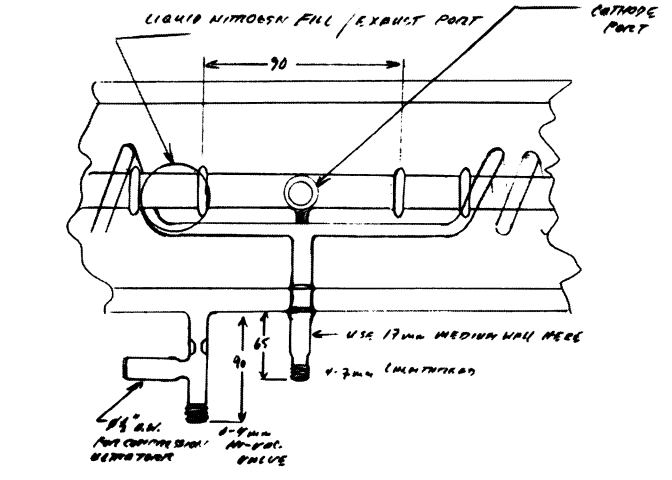

Final work at the middle of the liquid nitrogen reservoir involved forming the fill/exhaust port. This opening allowed the coolant to be added to the reservoir and was to be sufficiently large to allow exhaust from the coolant to escape around the supply nozzle. A small hole was opened initially. This left enough glass so that as the hole was tooled out with a graphite rod a sufficiently long extension was created which would later be sealed into and through the wall of the vacuum jacket. With holders left in position, the entire assembly was annealed at 560 degrees Celsius.

The ends of the coolant reservoir were completed next. The first end to be completed had its holder removed and the tubing inspected for debris from the graphite shims. All unused openings were plugged to allow air to be blown into and around the discharge tube (the cavity of the reservoir) which aided in the formation of the seals. Heat was concentrated on the reservoir tubing just to the right of the visible end of the discharge tube. After allowing sufficient glass to gather, the tube was rolled down and over the end of the discharge tube, fusing the two together with heat concentrated at the junction of the two tubes. The tailstock of the lathe was pulled away slightly to allow the excess glass to be removed from the seal. The end of the reservoir was given a hemispherical shape to enhance strength. The glass at the junction of the reservoir and the discharge tube was heated with a hand torch until a bubble could be blown out. Forceps were used to quickly grab the bubble while the flame of the hand torch "cut" away the excess glass. The opening formed was carefully tooled with a graphite rod to a diameter ready to receive a bellow.

While maintaining temperature on the end of the reservoir by directing a gas/air-annealing burner on the area, the tailstock was disengaged. One of the two expansion bellows, which were prepared previously, was quickly placed in the arms of the chuck ready to be fused onto the end of the reservoir. After re-engaging the tailstock, work was continued on the end of the reservoir. The bellow was carefully warmed in preparation to be sealed into place. An adequate seal was formed through a combination of heating, blowing and gathering by gently advancing the tailstock towards the end of the reservoir. Upon completion of a suitable seal, the entire area was slowly flame annealed and brought to room temperature before being furnace annealed. The same process was followed to finish the opposite end before the entire assembly was ready to be sealed into the vacuum jacket.

The annealed liquid nitrogen reservoir, complete with discharge tube and bellows, was then sealed inside the vacuum jacket. The jacket was prepared in the same way as the reservoir having bubbles blown out at locations where ring-seals would be formed for the liquid nitrogen port, the cathode port and the gas inlet port. At this time, the 4mm bore high vacuum valve serving as an evacuation port was sealed into position. Early completion of this feature helped to reduce working time in this region during the process of forming the necessary ring-seals for the other ports. The jacket was flame annealed, cooled and fitted with the liquid nitrogen reservoir. Care was taken to rest the assembled inner tube on cotton rags which were pulled like a "sled" across the inside of the jacket. All extensions to be sealed through the jacket had to be perfectly adjusted in length to prevent scratching the inner surfaces. Once in position, shims formed of glass fiber tape covered with graphite tape were gently positioned between the two tubes at each end. The center extensions for through seals were positioned up into the preformed bubbles.

Eight shims were used per end. The next step was to form the three ring-seals at the middle of the jacket.

Crucial to the success of completing the laser tube was patience in forming seals through the wall of the vacuum jacket opposite those already formed through the liquid nitrogen reservoir. Warming the area to be worked began with only a gas and air mixture from a Litton preheat/annealing burner. Gradually the flame temperature was increased with the addition of more air to the gas mixture until finally maximum temperature was achieved from the burner. This process took approximately thirty minutes. The seals that were already formed in the liquid nitrogen reservoir had to be warmed very slowly through the vacuum jacket to prevent cracks. The entire assembly turned slowly in the lathe throughout this process.

With the glass up to temperature, it was time to form the first of three seals in this region of the apparatus. The seals to the cooling coil tee, the cathode port and the liquid nitrogen fill/exhaust port were formed, respectively. Since each of the seals required connection to inner components, greater care had to be exercised in maintaining temperature on the area being worked, while at the same time not overheating the discharge tube allowing it to become distorted. (Some thought had been given to leaving the quartz straightening mandrel in place throughout the process. Satisfactory results were obtained without this procedure.) In this situation the annealing burner had been set up with a foot valve which maintained a pilot through the burner head. When seals were being performed, the burner was quickly turned off then reactivated immediately following short periods of work. This method proved successful at preventing any cracks due to thermal shock from premature cooling.

Seal quality in this area, as with the entire laser tube was essential to the success of the project. To assure the formation of adequate seals, each area of the jacket was thoroughly heated through until it fused into the tube extension from the coolant reservoir. Once the glass was softened adequately and the two areas flowed together, air was expelled into the cavity to help form the seal and bring back the distortion caused by the heating process. After the center of the seal became well-formed, a final heating was performed, concentrating the flame of the hand torch only within the ring of the seal. A bubble of glass was blown out. Forceps were used to quickly grab the glass and pull it away. In the same action, the flame of the hand torch continued to heat the glass as air blown into the seal eventually forced the glass to go thin and an opening was formed. The resulting hole was carefully tooled with a graphite rod ready to accept the diameter of the respective part. All of the external fittings were previously prepared enhancing the weight of the tubing stock at the sealing point. The cathode port, in particular, was prepared with an olive just above where it was to be joined to the laser tube jacket (figure 6). It prevented vacuum pressure from drawing the cathode inward towards the vacuum jacket through the compressed o-ring in the fitting. An earlier model of a liquid nitrogen cooled carbon monoxide laser was a victim of irreparable damage caused by the lack of such a feature.

With all of the seals completed at the middle section of the apparatus, the area was flame annealed and brought to room temperature. Before room temperature was reached though, the annealing burner was allowed to deposit a thick layer of carbon on the glass.

This insulation helped to further reduce the rate at which the glass cooled, and was considered an essential practice towards successful completion of the tube. All other work performed on the vacuum jacket received this type of treatment. The entire assembly was once again furnace annealed, leaving all supports in place.

Following the annealing process, the assembly was ready for shims to be removed from one end and final seals formed over the expansion bellow (figure 8). Once again, care was taken to load the tube in the lathe without damage. Steps were taken to line the lathe spindle with cotton rags to avoid scratches as the tube was inserted through. Support

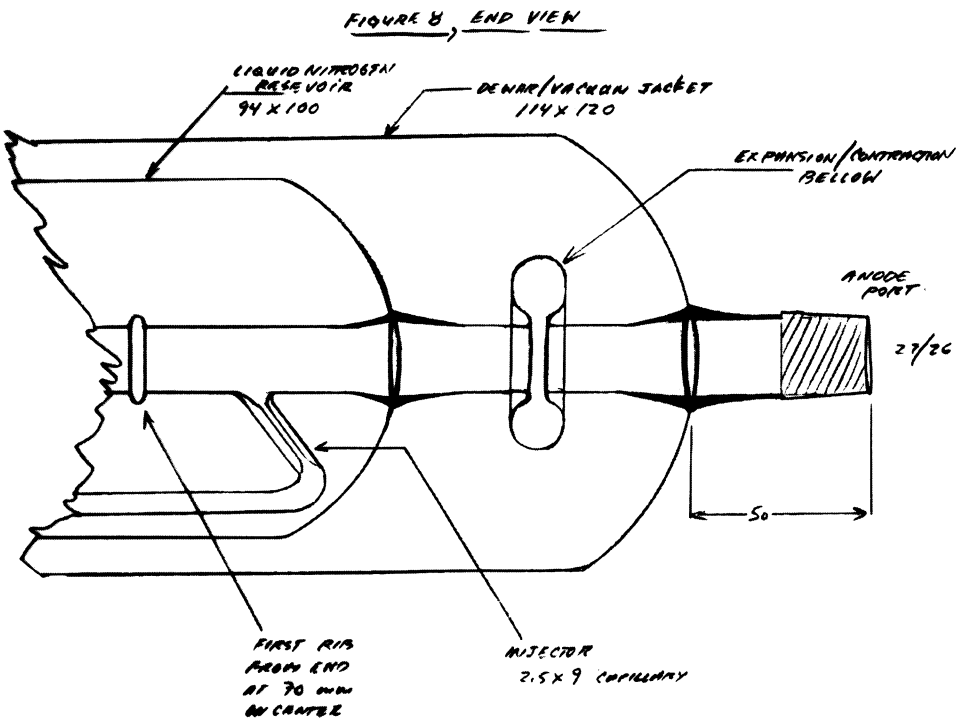

chucks at the backside of the spindle helped to support the weight of the apparatus. Once in place, shims were fitted to help the end of the tube run true. The tailstock held a scrap piece of tubing, which was used to connect to and pull away excess glass as the seal was formed. An inner member 29/26 was previously cut to length and set aside, ready to be sealed into place. Preheating of the area began with just methane and air and was progressively increased in temperature with the addition of more air pressure. This procedure took approximately thirty minutes. Heating of the jacket began just to the right of where the glass would eventually seal into the bellow. It was important to allow the glass to gather a bit before the tailstock was pulled away. Also, heat of the burner had to be controlled so as not to overheat the bellow, which would begin to move out of alignment. The lathe was never stopped throughout this seal. Once the glass was pliable, it was tooled down and over the end of the bellow. Forming the hemispherical end as the glass was tooled down reduced the need to reshape the area once the glass was closed over the bellow. A tremendous amount of heat was concentrated on the seal to assure

strength. It was opened to accept the 29/26 joint in a manner not unlike the seal formed with the liquid nitrogen reservoir discussed earlier in this paper. The 29/26 joint was sealed into place having the glass gathered near the ring of the seal and progressively tapering off to the weight of the joint stock. The length of the part from the seal was adjusted to within specifications before the flame annealing process began. Once again, the area worked was brought to room temperature very carefully leaving a layer of carbon to insulate it against thermal shock. The entire tube was then annealed. The opposite end was finished in the same manner before a final annealing of the finished apparatus was performed.

Remaining work to fabricate a liquid nitrogen cooled carbon monoxide laser involved constructing a cathode and two anodes. The cathode was designed using glass compression fittings (figure 9). Two fittings sealed together formed the body of the adapter. A smaller fitting, sealed perpendicular to the larger tube, formed the seal around the electrode and held the stainless steel component in place. The electrode was threaded on one end to make a connection. A leak-tight connection through the compression fitting was only possible with a polished rod having no surface pits or scratches.

FIGURE 9, CATHODE

QUANTITY 1

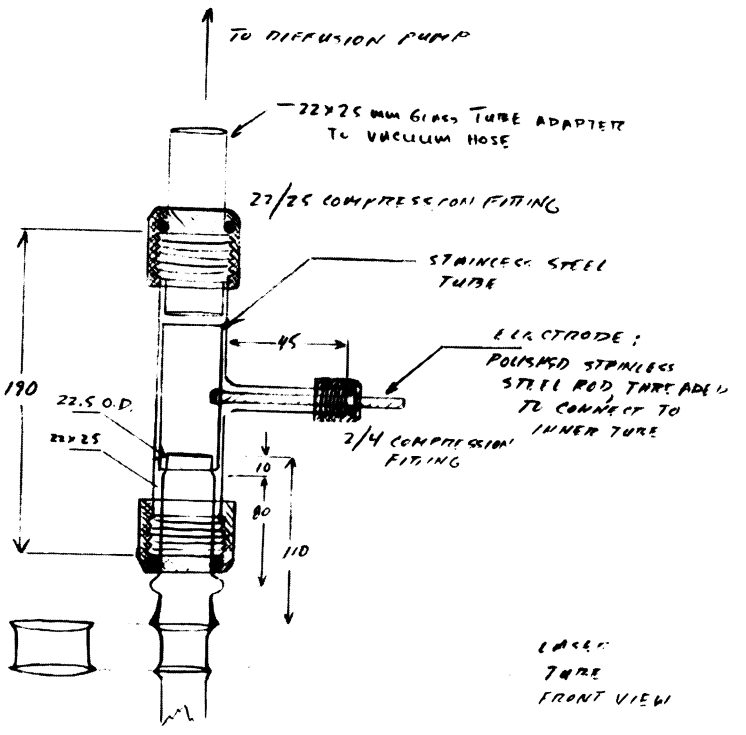

The anodes were formed off of 29/26 outer member ground glass joints (figure 10). Two were needed. The desirable orientation was to have the electrode arms of the anodes on the same side of the laser tube when in place. All other details were the same for both orientations. Adapters were formed with three different size glass compression fittings to accommodate the different diameters of the component parts. The open end of the adapter accepted a gas feed tube. The perpendicular arm supported and sealed into place the electrode which was designed with a threaded connection into the wall of the stainless steel excitation tube. The entire adapter mounted onto the side arm of the anode. A section of tubing having an outside diameter of 22-millimeters was added to each ground glass fitting. The ends were cut to Brewster angles. Optical windows were fixed in place with epoxy.

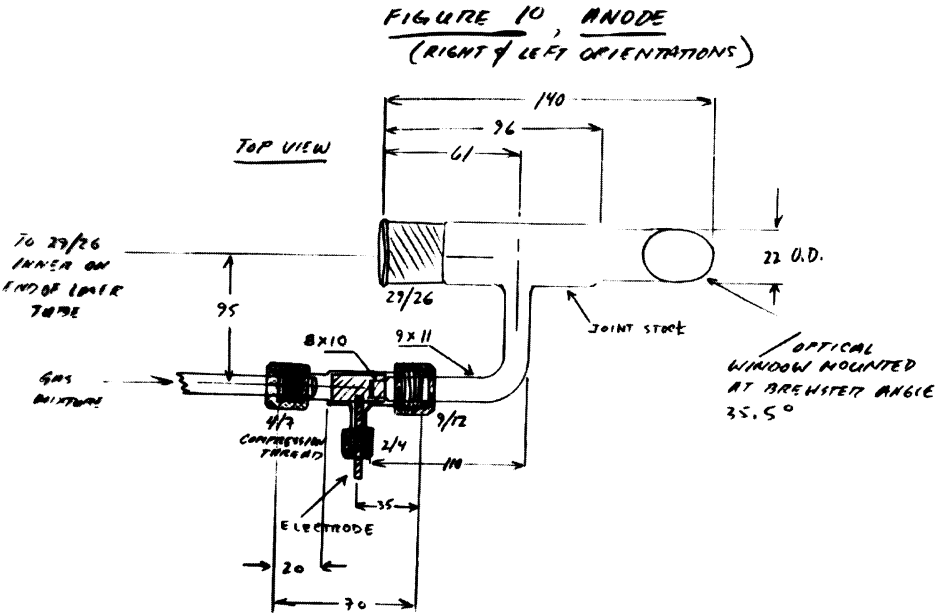

In conclusion, the 1000-millimeter liquid nitrogen cooled carbon monoxide laser tube discussed in this paper has performed without failure since its completion. The modifications introduced improved the user-friendliness of the apparatus. No accidents or damage to the tube have been reported since threaded glass compression fittings were used in place of ground glass fittings. Threaded glass fittings replacing glass-to-metal seals on the cathode and anodes have performed well. There was a concern that heat generated from electrical current would damage the o-rings in the seals, but this was never observed. The dynamic vacuum applied to the dewar proved effective at insulating the liquid nitrogen reservoir. Unlike tubulated jackets on other tubes, there was very little condensation build-up on the exterior of the laser tube; this allowed for an uninhibited view of the discharge over extended periods of operation.

Improvements in the fabrication process might include using a mandrel to support the discharge tube throughout the different annealing stages. Use of a graphite mandrel may reduce the chance of accidental damage. Also, incorporation of some glass supports may aesthetically improve upon coils sagging throughout annealing stages. This was reduced to some extent by rotation of the tube assembly, positioning the "high side" of the coil

up and allowing it to fall back towards its original position. Only slight distortion was observed after the final annealing stage.

Notes

[A] Anthony E. Siegman, Lasers, Mill Valley (CA: University Science Books, 1986).

[B] S. Bürscher, O. Schultz, A.Dax, H. Kath, and W. Urban, "Improvement of the Performance of cw CO Lasers Using Externally Ribbed Wall Cooled Discharge Tubes," *Applied Physics B* Vol. 64 (1997): 307-309.

[C] Michael John Grassi, "15W High-Efficiency Liquid Nitrogen Cooled Fast Axial flow Electrical Discharge CO Laser Operating Single Line," Master's Thesis, Ohio State University, 1993

[D] Matthew Douglas Chidley, "Design and Operation of a Dual Co Gas Laser System for the Optical Pumping of a Large Volume Plasma," Master's Thesis, Ohio State University, 1999.

Glass Cells for Neutron Spin Filters Using Polarized ^{3}He

by
F. William Hersman, Ph.D.
Physics Department
University of New Hampshire
Durham, New Hampshire 03824

ABSTRACT
Polarized helium-3 cells have been used successfully to polarize beams of low energy neutrons. The polarized helium-3 nuclei capture neutrons whose spin is oppositely directed, while allowing those with the same orientation to pass through. The constraints of alkali resistance, helium permeability, and neutron transmission require special glass formulations, surface treatments, and/or new cell designs in order to fabricate neutron spin filters for an upcoming nuclear physics measurement at Los Alamos.

Neutrons and nuclei

Neutrons, together with protons, are the basic building blocks of atomic nuclei. They are exceedingly small, having mass of 1.67×10^{-27} kilogram, and size of 0.8 femtometer (10^{-15} meter). While they have no electric charge, they nevertheless have a small magnetic moment, associated with their spin. Polarizing neutrons consists of aligning the spins (more-or-less) along a particular direction and holding their orientation with a magnetic field. Neutrons have a mean lifetime of only 15 minutes before decaying into protons (and other particles). Consequently, they must be used shortly after and in close proximity to where they are produced.

Free neutrons are produced for physics experiments primarily by one of two methods. A source of neutrons that is continuous in time can be obtained from a nuclear reactor. Alternatively, a source of neutrons that is concentrated in bursts can be obtained by using a particle accelerator to knock lots of neutrons out of a thick block of material. This process is called neutron spallation and is required for the experiments I discuss today. The advantage of this method is that fast neutrons arrive at our experiment shortly after the burst of particles comes from the accelerator, while slow neutrons arrive much later. We can determine the velocity of the neutrons based on how much time separates the beam burst and the neutron's arrival at our experiment.

Spallation produces large quantities of neutrons for study. At the Los Alamos Neutron Science Center (LANSCE) the spallation source produces about 12×10^{13} neutrons per second per each eV energy bin. Most of these are going in unusable directions, and get absorbed onto the shield. Nevertheless, roughly ten billion per second go into our 10 cm x 10 cm beam line and get directed to our experiment.

Most of the helium in the world has two protons and two neutrons, for a total of four, hence the moniker ^{4}He. We are interested in using ^{3}He, which has only one neutron. Since the two protons cancel each other's spin and magnetism, the single neutron provides the

spin and magnetism for ^{3}He. If another neutron comes in the vicinity with spin (and magnetism) directed opposite to the ^{3}He nucleus, it is absorbed with high probability (Figure 1). On the other hand, neutrons with their spin oriented in the same direction as the ^{3}He nucleus are 700 times less likely to be absorbed: they pass through. Consequently, a glass cell filled with polarized ^{3}He gas acts as a spin filter for neutrons: it allows neutrons with parallel spin orientation to pass through and absorbs neutrons with the opposite spin orientation.

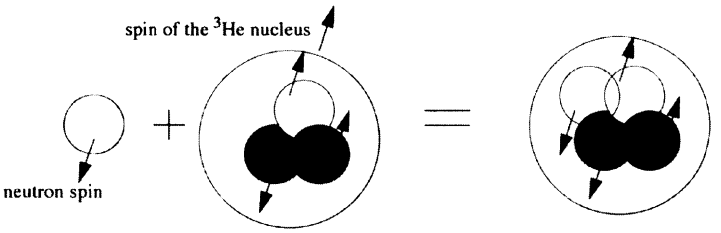

Figure 1. Neutrons with their spin directed opposite to that of the ^{3}He nucleus are absorbed with much higher probability.

Why polarize neutrons?

Polarized neutrons are being used in applied and basic research. The primary application of polarized neutrons is to study the atomic and molecular structure of the magnetism in solid materials. Our collaboration, however, is planning to use polarized neutrons to measure details about parity violation, a fundamental property of one of the forces of nature.

The forces of nature that are most familiar are electricity and magnetism, and gravity. Less familiar are the two nuclear forces, sometimes called the strong and weak nuclear forces. The weak nuclear force is the only one known to violate parity. This peculiar property has important origins in the evolution of the universe after the big bang.

The parity operation is a lot like reflection in a mirror. Some objects may look the same reflected in a mirror (spheres, cubes) while others look different (the alphabet). Up until the 1950's, physicists thought that all the laws of physics would behave the same if everything involved in the process were reflected in a mirror. In particular, processes that involve two orientations because they depend on a direction of travel (momentum) and a rotation (spin) could in principle behave differently, since reflection in a mirror will reverse only one of those directions, not both. An example would be if you weighed more (and therefore dropped faster in gravity) if you were spinning to your left rather than spinning to your right. Obviously this is not the behavior we observe for gravity. In 1956, Professor C. S. Wu measured a particular nuclear radioactive decay and found an excess of particles emitted with momentum along the direction of the nuclear spin, a violation of parity attributed to the weak nuclear force. Our experiments are extensions of that Nobel prize-winning discovery.

Polarizing helium-3

The process we use for polarizing the ^{3}He nucleus involves polarizing the electron on a rubidium atom. A very pure, closed glass cell containing helium gas, rubidium metal, and a small amount of nitrogen is prepared. This cell is warmed to 180°C to cause some of the rubidium metal to become vaporized, and placed in a magnetic field that can hold the spin direction. A laser is adjusted to produce light at a wavelength of 794.7 nm, in the infrared region just beyond the visible red region. This is the wavelength that can be absorbed by the rubidium atoms. The laser light is passed through special optics that

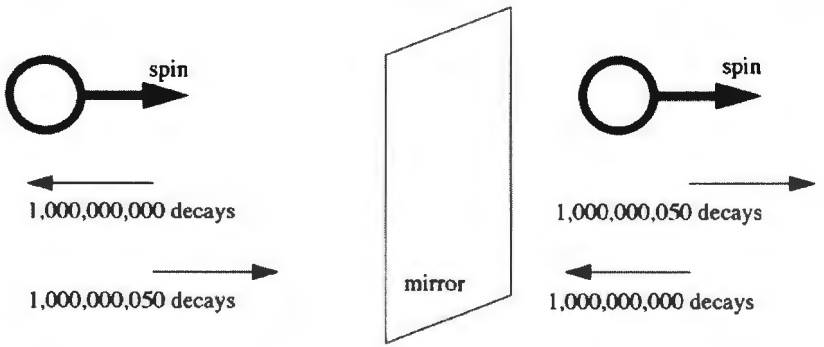

Figure 2. A parity violating reaction: if more particles are emitted along the direction of the spin, then the process looks different if reflected in a mirror.

polarizes the light in a circular pattern (like a corkscrew). If a rubidium atom absorbs this light, its electron will become polarized, that is, its spin will point in a particular direction (along or against the magnetic field). In a fraction of a second, essentially all the rubidium atoms have electrons that are polarized. These electrons exert a very small torque on the ^{3}He nucleus when the atoms collide, causing it to orient along the same direction. After a period of several hours to several tens of hours, most of the ^{3}He nuclei can become polarized along the direction of the rubidium electron spins.

Figure 3. Dan Hussey poses for a picture, pretending to check on the bake-out of a glass cell enclosed by oven bricks.

The ^{3}He polarizing process imposes requirements on the enclosing cell. The efficient absorption of the laser light depends not only on the rubidium density, but also on the helium pressure. This is because the helium pressure will cause the process to work not only at a wavelength of 794.7 nm but also at nearby wavelengths (down to 793.7 nm or up to 795.7 nm). Since the laser produces light spread over these wavelengths, this light will be wasted if there is not sufficient helium pressure. The cell should be transparent, allowing the polarized laser light to pass through to the rubidium vapor. It should not be birefringent (unless corrections can be made). It should be alkali resistant and impermeable to helium leakage.

Neutron spin filters

Neutrons emitted from the spallation source and travelling in the direction towards the experiment have randomly oriented spins. In the presence of the magnetic field that holds the ^{3}He polarization and defines a direction, half of the neutrons are oriented parallel to the ^{3}He nuclei and the other half are antiparallel. As the neutrons travel through the polarized ^{3}He gas, the parallel neutrons are transmitted more favorably while the antiparallel neutrons are absorbed. Consequently, more neutrons emerge with their spins parallel to the polarized ^{3}He (Figure 4).

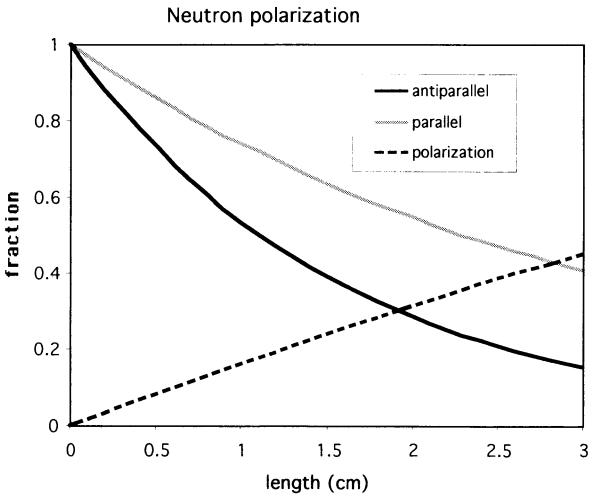

Figure 4. Absorption and transmission of neutrons with their spins oriented parallel and antiparallel to a sample of ^{3}He with polarization of 40% and pressure of three atmospheres.

The neutrons must enter and exit the cell, which holds the helium. This imposes additional constraints on the cell materials and properties. The cell must cover the area of the neutron beam uniformly. There must be sufficient thickness and polarization of the helium gas to accomplish the task of polarizing the neutrons, but not so thick so as to absorb all the neutrons. The glass should be transparent to neutrons, allowing them to pass without significant absorption or polarization change.

Constraints and difficulties

The constraints described above can be summarized and compared with existing capabilities and materials. The conditions imposed by the requirements for polarizing helium, including the resistance to alkali metal vapor, could be confined to a polarization region. Aluminosilicate has excellent resistance to heated alkali vapors. The region where the neutrons pass through could then be made of a different material.

Transparency to laser light points to glass, at least for the laser light entrance. Low permeability to helium should be satisfied by the entire cell, unless there is some way to replace helium. Aluminosilicate has an extremely low permeability, borosilicate is one hundred times worse, and quartz is terrible. It is possible that coatings could improve the helium permeability of quartz.

The nuclei of ^{3}He will depolarize if they come in contact with any atoms with magnetism, if they stay in contact with the surface for all but the briefest of collisions, either because they got stuck or burrowed into the surface. Glass compositions containing iron or surface impurities of oxygen are known to prevent long polarization storage times and high polarizations. Aluminosilicate which is formulated without iron and prepared from purified iron-free components has been shown to be excellent. High temperature bake-out seems to remove most oxygen-containing surface impurities. Most glass contains boron. Normal boron is 20% boron-10 and 80% of boron-11. Unfortunately boron-10 is highly absorptive of neutrons, 700 times more than boron-11. The neutron cell must be prepared from boron-free glass, or glass made using isotopically pure boron-11.

Our best so far

Participants from several labs and universities joined together in the TRIPLE Collaboration to produce polarizing cells and perform experiments with polarized neutrons. Flat windows were prepared from various aluminosilicate materials and joined to cylindrical bodies. The cells were baked out at 350°C and filled with 100 torr of pure nitrogen, doubly purified ^{3}He gas, and doubly distilled rubidium metal. The polarization storage times ranged from 40 hours to over 80 hours. Three of these cells were used in successful experiments at LANSCE (Figure 5).

Cell	Dia. × Length (cm)	P (273K)	Γ-1 (hr)	windows
LA2	3.4 × 10.0	3.0 atm	84.3	2 mm 1723
LA5	3.6 × 10.0	4.8 atm	48.5	3 mm 10B and Fe free 1720
LA7	3.4 × 10.0	5.5 atm	38.1	3 mm 10B and Fe free 1720
LA12	3.6 × 10.1	5.6 atm	47.3	3.2 mm Fe free 1720
LA13	3.6 × 10.0	5.5 atm	41.1	3.2 mm Fe free 1720

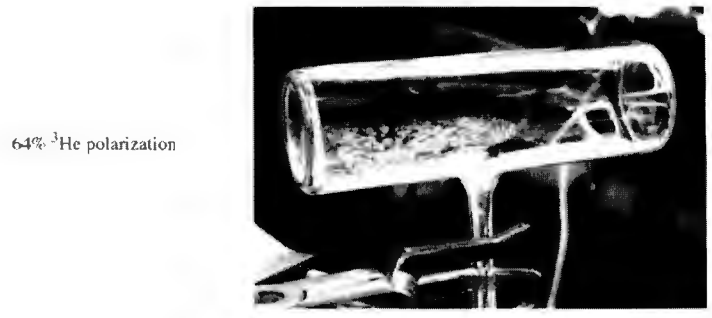

Figure 5. Cell LA2 was used to produce a beam of 40% polarized neutrons

New requirements for n p $\rightarrow$ dγ

The first of a new generation of polarized neutron experiments is now posing requirements that stretch our current capabilities. In this new experiment, polarized neutrons are captured by protons to make deuterons and emit gamma-rays. An excess of gamma-rays along (or against) the direction of the neutron spin would violate parity, as is expected due to the weak nuclear force. The advantage of this experiment over previous experiments is that the process involves the simplest nuclear particles: a proton and a neutron. The difficulty is that the expected parity violation is only fifty extra photons for every billion that are emitted. We will need around a billion-billion neutron-proton interactions to make an accurate measurement. That means we need the biggest beam line, the biggest proton target, and the biggest neutron spin filter we can possibly make.

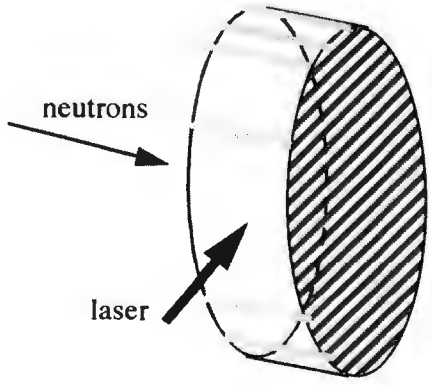

Figure 6. Schematic layout of the upcoming n p $\rightarrow$ dγ experiment at LANSCE.

We have designed the apparatus assuming a 4" x 4" beamline. This requires either a 4" x 4" square or a 6" diameter neutron spin filter cell. We have estimated that the experiment is performed best if there is an amount of helium in the pathway whose density-times-thickness is 4 to 6 atmosphere-cm (@273K) This is relatively thin, especially when you account for the fact that the pressure should be significantly greater than one atmosphere in order to make efficient use of the laser light. Finally, we will need to run the experiment for a year or more, even with these large dimensions. Reducing the size of the apparatus will require a longer running time. It is obviously desirable that the cell should operate without failure for a long time.

Current efforts are approaching this design problem from a number of approaches. The simplest conceptually would be a single high pressure cell, with a sufficiently large diameter. The entire cell would be heated and contain rubidium vapor. The pressure would be approximately two to three atmospheres with the thickness in the range of 2 cm to 3 cm. The laser light would enter the side, illuminating the entire 15 cm x 2 cm rectangular cross section. Experimenters at NIST began by exploring this design.

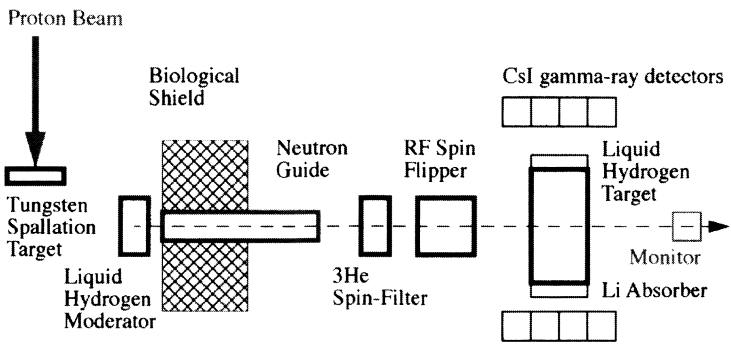

Figure 6. Schematic design for a single cell polarized helium neutron spin filter.

Most of the various remaining approaches separate the ^{3}He polarizing cell and neutron spin filter cell. The simplest of these would place a 1" diameter cylinder of several inches length off to the side for polarizing the ^{3}He. This cigar-shaped cylinder would be in a warm enclosure for vaporizing the rubidium. The polarized ^{3}He would diffuse through a connecting tube into the neutron polarizing cell, which would be at room temperature and similar in geometry to the pancake-shaped disk shown above.

The simplest of the two cell designs would use aluminosilicate glass for both cells. In this case, only the geometry has changed to allow more ideal overlap with the laser beam and the neutron beam. The large flat windows must be boron-free, while the entire volume should either be iron-free or coated (to minimize helium depolarization). Alternatively, they could be made of different materials, solving some problems and creating others. If the rubidium is confined to the polarizing cell, then only that cigar-shaped cell needs to be alkali resistant. The pancake-shaped neutron spin filter cell could be made of quartz, which is easier to fabricate and free from neutron absorbing impurities. Unfortunately quartz leaks helium. This problem could be addressed three ways. The first would be to simply tolerate the leakage and replace the cell when the pressure drops. The second would be to attach a valved cell and replace the lost helium periodically. The

third would be to develop a sol-gel coating for the quartz that reduces or eliminates the leakage. These approaches are being explored at the University of Michigan, NIST, Princeton, and the University of New Hampshire.

Summary

Neutron spin filters offer new paths to discovery. The high polarization that is achieved for very large quantities of neutrons for a large range of velocities opens possibilities that were not available before. Still, each improvement we are able to achieve in helium polarization, and the accompanying improvement in neutron polarization, lowers the cost of these multi-million dollar experiments. Consequently, we will always be pushing the limits of glass materials and techniques. Furthermore, as improvements emerge and become routine, even more creative and ambitious experiments will be envisioned and proposed. What has been true for hundreds of years remains true today: the advance of science vitally depends on our understanding of the material properties of today's glass and the techniques and skills of today's glassblowers.

Introduction to Centerless Grinding and Polishing of Glass

by
Philip M. Rossi
Precision Electronic Glass, Inc.
Vineland, New Jersey 08360-3295

This presentation is meant for the curious person with no centerless grinding experience. The intent is to provide you with the basic principles of centerless grinding as it relates to the glass industry. This presentation will not make you an experienced centerless grinder but it will instill you with the basic principles of this simple but, at the same time, complex process.

It is important that you first understand that all glasses are not of the same composition. Considerable experience is necessary to adapt the principles of grinding to these vastly differing materials we call glass.

Let us start with the definition of centerless grinding (photo 2):

- Centerless grinding is the precision grinding of the outer surface of a cylindrical part.
- The work piece is supported without regard to the center axis of the part.
- In centerless grinding, the work is supported on a work-rest blade between the regulating wheel which controls the speed of grind and the grinding medium whether it be a wheel or a belt.
- The regulating wheel serves as both a driving wheel and a brake, rotating the work at a constant speed.
- There are two types of centerless grinding machines that are commonly used in the glass industry. The first machine uses a rigid grinding wheel and the second uses a grinding belt.

Photo 2. Centerless Grinding
The precision grinding of an outer surface of a cylindrical part. The work piece is supported without regard to its center.

The elements of centerless grinding (drawing 3):

- Grinding wheel turns into work at a high rate of speed.
  - Typically made of silicone carbide for glass grinding.
- Regulating wheel.
  - The speed and angle of the regulating wheel control the speed at which the work passes through the machine.
  - The regulating wheel is typically a rubber bonded abrasive wheel.
- Work-rest blade.
  - Supports the work piece between the wheels.
  - The blade is adjustable in height to raise or lower the height of the work in relation to the wheels.
  - The top edge is usually made of hardened steel or carbide to minimize wear. When visibly worn, the blade can be redressed.
  - The top edge is typically at a 30° angle so that the downward pressure of the grinding wheel tends to push the work away from the grinding wheel and towards the regulating wheel.
- The work piece, as it sits on the blade and between the wheels, rotates at the surface speed of the regulating wheel.

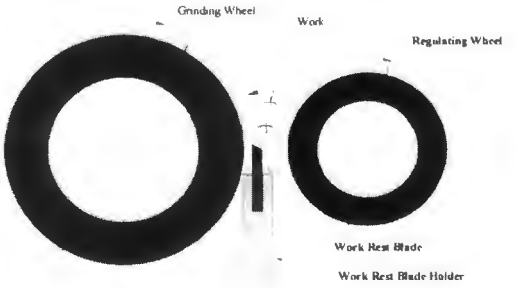

Drawing 3. Principles of Centerless Grinding

Let us now discuss the three types of centerless grinding (drawing 4).

Through-feed centerless grinding:

- Drawing 4 is of a typical part that could be centerless ground.
- Straight cylindrical parts pass from the entrance across the wheels (or belt) and out the exit of the machine.
- The grinding and regulating wheels are set at a slight and increasingly narrow angle.
- This is a continuous process where parts of a single diameter are fed into the machine one after another.
- The process removes excess material as the parts pass through the wheels, resulting in the parts being ground to a precise diameter.
- The rate of feed is highly dependent on:
  - Diameter of work.
  - Type of material.
  - Amount of material to be removed.
  - Tolerances to be met.

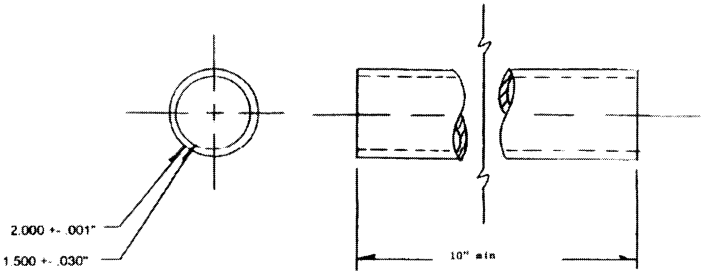

Drawing 4. Through-feed Centerless Grinding

In-feed or plunge centerless grinding (drawing 5):

- This drawing shows a multi-diameter part that can be plunge ground.
- Typically a part is placed between the wheels against a stop and the operator will either pull a handle or engage an hydraulic drive that brings the regulating wheel towards the grinding wheel. This allows the grinding wheel to gradually remove the excess material.
- This is used when the shape does not allow the part to pass entirely through the machine. Also, the part usually has a shoulder or head.
- Multiple diameters may be ground at one time.
- The length of the grind is limited to the width of the wheels as there is no axial movement of the work.
- Special dressing attachments may be required depending on the profile of the completed part.

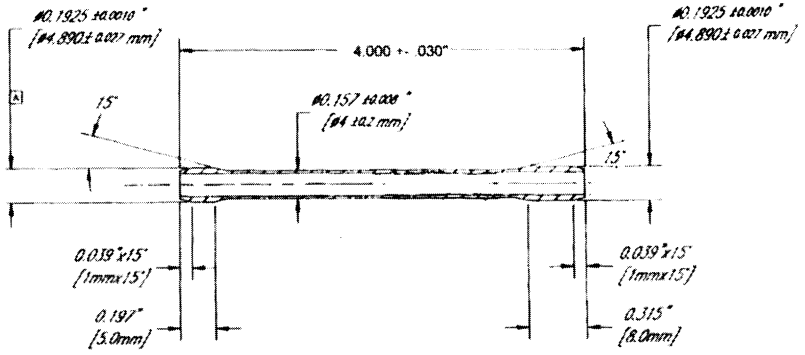

Drawing 5. In-feed (Plunge) Centerless Grinding

The third type of centerless grinding is called "End-Feed" centerless grinding (drawing 6):

- Drawing 6 depicts a taper which is quite typical for end-feed grinding.
- This method is used to produce tapered parts.
- The part is fed into the entrance of the machine and the part travels to a fixed stop.
- The grinding wheel, regulating wheel and work rest blade are set in a fixed relationship to each other so as to create the desired taper.

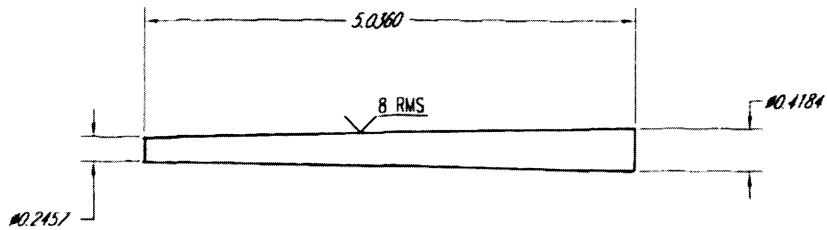

Drawing 6. End-feed Centerless Grinding

Photo 7 shows a piece of metal being centerless ground. There are two types of centerless grinding machines commonly used in the glass industry. This is a centerless grinder with a rigid wheel.

Why a rigid wheel?

- Better dimensional stability.
- Lower cost to grind due to life of wheels.
- Can hold very tight tolerances +/-.02% per inch of diameter (.0002" per inch of diameter).

Disadvantages:

- Relatively high cost of machines.
- Long set-up times.
- Not practical to change the grinding wheel on a frequent basis thus limiting the machines' range of use.
- High wheel cost.

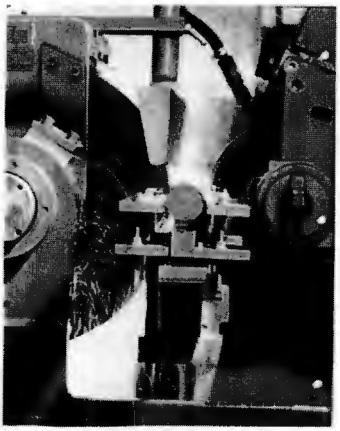

Photo 7. Centerless Grinding with Rigid Wheel.

The second type of grinder used is a belt centerless grinder (drawing 8). Unlike a rigid wheel, these machines use a grinding belt. Belt machines have become very difficult to locate in recent years and the prices of new and used machines have risen. Note that the belt travels at 10,000 SFPM (surface feet per minute).

Advantages of belt:

- Belts can be quickly changed allowing for a continuous flow to progressively finer belts.
- Glass can be polished.
- More aggressive grinding.
- Ease of set-up.
- More forgiving of out-of-round material and bowed material.

Disadvantages:

- Less accurate than the rigid wheel +-.05% of diameter (.005" per inch of diameter).
- High cost of grinding due to short belt life.

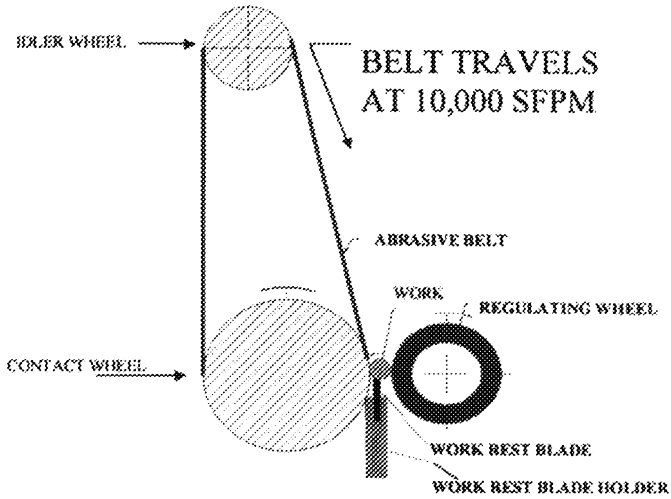

Drawing 8. Centerless Belt Grinder

In order to make parts round in the grinding process, the most important factor is the location of the work as it relates to the centerline of the grinding and regulating wheels.

Grinding on center:

- To grind work cylindrically (round), the height of the work piece is adjusted by raising or lowering the work rest blade so as to place the center of the work above the centerline of the wheels. The height varies based on the diameter of the work and ranges from an amount equal to 1/2 the work diameter to a maximum of 1/2" above center.
- The height of the centerline of the work in relationship to the centerline of the wheels is directly proportional to the part roundness after grinding. The higher the part is held above center, the rounder the result.

- Drawing 9 shows a part being ground on center.
  - The two wheels and the blade form 3 sides of a triangle.
  - As the work is rotated and the high spot comes in contact with the regulating wheel, the part will be pushed into the grinding wheel causing a diametrically opposite low spot.
  - This set-up will NOT produce a round part.

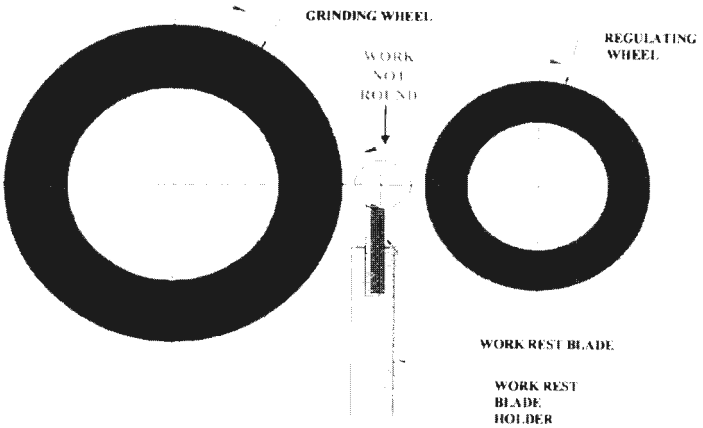

Drawing 9. Results of Grinding On Center

Grinding above Center (drawing 10):

- When the center of the work piece is above the wheel centerline, any high spot coming in contact with the regulating wheel will push the work into the grinding wheel creating a low spot that is not diametrically opposite the high spot. (The high and low spots are not opposite each other.)
- As the work is rotated, the high and low spots do not occur opposite each other as they do when a part is ground on the centerline of the wheels and gradual rounding takes place.
- The rounding action is also increased by a high working speed and a slow rate of through-feed.
- If work is too high, it will chatter as there is not enough downward force to keep the work on the workrest blade.

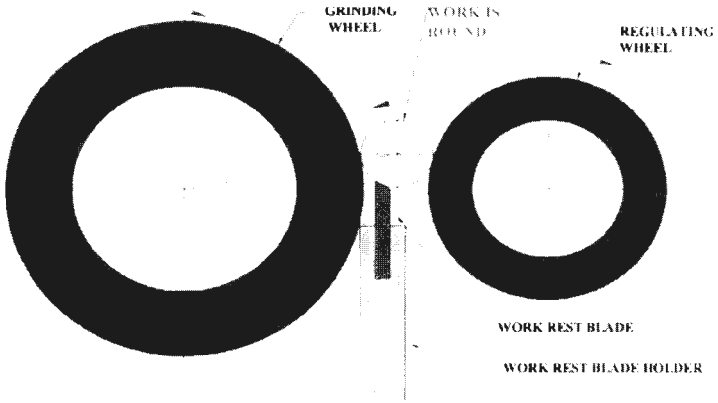

Drawing 10. Grinding Above Center

Both the grinding and regulating wheels require dressing with diamond tools. This dressing ensures that the wheels are in proper contact with the work. Skill and experience are critical to success in centerless grinding. Here are some common problems that occur:

- Dressing of the regulating wheel is critical to the result of the part. An improperly trued regulating wheel, will result in a concave face and will produce parts that are hour-glass shaped. Dressing the wheel with a concave face will produce a barrel shape (drawing 11).

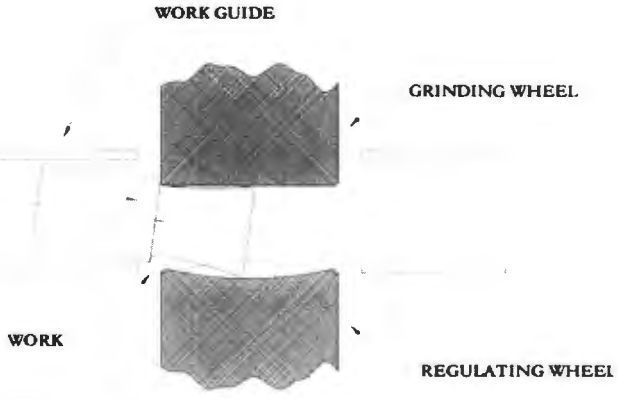

Drawing 11. Results On Part of a Concave Regulating Wheel

Machines typically have work guides on the inboard and outboard sides of the machines. The purpose of the guides is to keep the work properly aligned. Improper alignment may result in a number of problems.

- When guides are improperly aligned to direct the part of the grinding wheel, a spool shape (narrow center) will be the result (drawing 12).

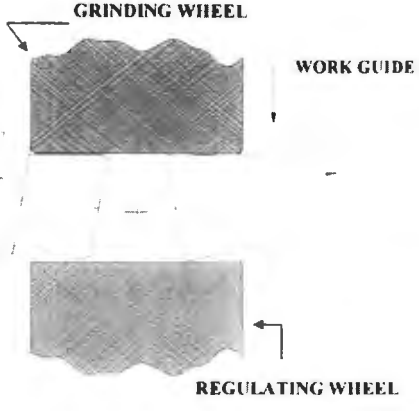

Drawing 12. Hour Glass Shape Due to Improper Guide Alignment

• When the guides are improperly deflecting the work toward the regulating wheel, a barrel shape will be the result (drawing 13).

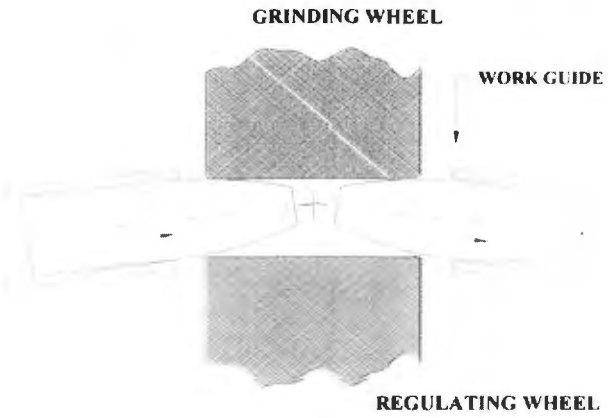

Drawing 13. Barrel Shape Due to Improper Guide Alignment

Whether centerless grinding with a rigid wheel or a belt, the setup is the key to success. Other common problems that can occur:

•Chatter: Work too high above center or wheel too hard.
• Erratic Sizing: Machine out of adjustment.
• Out of Round: Part not high enough above center.
• Spiral Chatter: Exit guide too far forward or sharp or chipped edge at exit side of grinding wheel.
• Taper: Work rest blade on angle.

The straightness of the material being ground plays a major role in the grinding process. These are only a few of the more common problems associated with centerless grinding. I have enclosed a troubleshooting guide from Cincinnati that is more inclusive.

Centerless grinding wheels for glass are generally made of vitrified silicon carbide. The vitirifed bonding is a glass-like material that is used for higher precision requirements. The bonding holds the abrasives in the proper angle for grinding (chart 14).

To correctly determine the composition of the grinding wheel, considerable experience is required. Many factors must be taken into consideration when choosing a wheel:

• Material to be ground.
• Diameter to grind (includes stock removal).
• Type of grinding (Through-feed, in-feed or end-feed).
• Finish required.
• Parts between dressing.

There are no absolute rules for choosing the wheel, so experience or trial and error are the norm.

Grinding Abrasives

The most common abrasives used in centerless grinding.

- Aluminum Oxide
  -Soft material that is usually avoided in glass grinding due to cost and availability.
- Silicon Carbide
  -Most commonly used in glass grinding
- Diamond
  -Generally too expensive for centerless grinding.

Chart 14

Abrasive belts are commonly used in the glass industry. The construction of a belt is more than meets the eye. An abrasive belt has 4 to 5 elements:

- Waterproof backing material (Base).
- Glue coating (Binder).
- Sizing coat.
- Mineral grains (Abrasive).
- Top coat (for some types).

As in grinding wheels, there are many factors to consider in the belt. Of significant importance are the following:

- Quality of the abrasives (belt life and cutting ability).
  - This includes even grain sizes in the belt and orientation of abrasive grain (vertical to the axis of the belt surface).
- Splice
  - Belts start off as a continuous sheet (jumbo) and are transformed into belt by converters.
  - There are a number of different splices available but a weak or uneven splice will affect belt life.

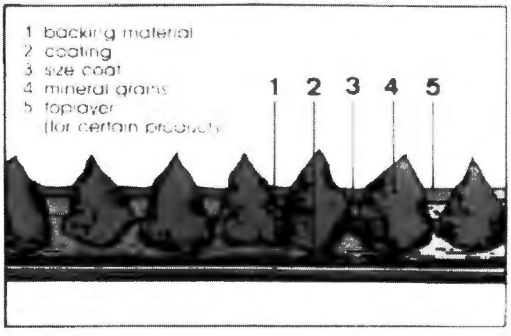

Chart 15. Abrasive Belts

The material of choice for polishing on a centerless belt grinder is cork. Cork comes from The Cork Oak Tree (photo 16).

This is a Mediterranean evergreen tree,, which grows primarily in Spain and Portugal. The bark is rugged, thick and spongy, pale grey or brown, and deeply fissured. When the tree is 20 years old, the outer layer of bark can be stripped (1-2" thick by about 9 feet long) leaving the reddish-colored trunk exposed. Every 8-10 years thereafter, the bark can be stripped again. The tree will regenerate the bark for about 150 years. The cork is ground and applied to the belt material using the same process as abrasive belts.

Photo 16. Cork Oak Tree

Glass Polishing:

The grinding process is carried out in stages using progressively finer abrasives to prepare the surface for polishing. Luster and transparency are obtained by cork polishing. Glass polishing success is highly dependent not only on polishing methods but also on the preceeding grinding operations. During polishing, material is no longer removed from the diameter. Under the pressure of the polishing medium (cork), the outer surface of the glass melts for a microsecond. Grinders see this occurrence as a line of fire (photo 17).

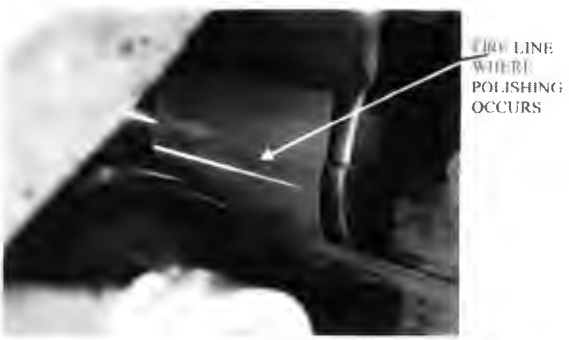

Photo 17. Cork Polishing On Belt Grinder

Multiple passes may be required depending on the diameter of the work and the polish desired. Cork polishing will leave a slightly cloudy appearance and a final polish of cerium oxide can be performed after the cork polishing to return the glass to its original clarity.

Surface finish comes in many varieties. Chart 18 allows you to convert from different standards that may appear on a print. Most commonly used is the Ra and we consider any finish ≤16 to be polished.

MICRO ENGINEERING CONVERSIONS

Surface Roughness

Ra (μin.)	1	2	4	8	16	32	63	125	250	500	1000	2000
Ra (μm)	.025	.05	1	2	4	8	1.6	3.2	6.3	12.5	25.0	50.0
RMS (μin.)	1.1	2.2	4.4	8.8	17.6	35.2	69.3	137.5	275	550	1100	2200
Rt (μm)	3-4	5-7	9-11	15-20	23-28	5-6	10-12	16-20	30	50	100	200
N Values	N1	N2	N3	N4	N5	N6	N7	N8	N9	N10	N11	N12
Swiss Stds	▽▽▽▽			▽▽▽				▽▽			▽	

Dimensional

1 Microinch = 1μin. = 10^{-6} in. = 254Å = 25.4nm = .206 seconds per inch
1 Micrometer = 1 micron = 1μm = 10^{-6} meters = 10^{4}Å = 39.37μin.
1 Nanometer = 10^{-9}meters = 10Å = 3.937×10^{-8}in.
1 Angstrom = 1Å = 10^{-10}meters = 0.1nm = 3.937×10^{-9}in.

Chart 18. Micro Engineering Conversion Chart

References:

As this has been a very basic introduction, I would recommend some of the materials that I have referred to over the years.

Bukart, W., and K. Schmotz. Grinding and Polishing Theory and Practice. Redhill, England: Portcullis Press Ltd., 1981.

Grinding Wheel Application Guide. Cincinnati, OH: Cincinnati Milacron Marketing Co., 1983.

Micro Engineering Conversion Chart. Adison, IL: Surface Finish Co., n.d.

Investigating Bubble Formation in Butt Seals with the Aid of an Electron Microscope

by
Hans Rohner
University of Colorado - JILA
Boulder, Colorado 80309-0379

Abstract: This paper describes observations of saw cuts in quartz and borosilicate glass with both silicon carbide and diamond wheels. I show which surface topology is prone to bubble formation in subsequent butt joints. The observations are largely phenomenoligical, with minimal theoretical speculation as to why the bubbles form.

Introduction: Glassblowers have long observed that borosilicate and soft glasses, when cut with a silicon carbide abrasive wheel and left unetched, will form a line of bubbles at the joint when subsequently sealed. Quartz does not suffer the same defect under similar procedures. When diamond abrasive wheels are used instead of silicon carbide, the bubble formation at the seal is as good as eliminated in the borosilicate glasses as well.

The wheels used in the investigation are 14" diameter 120 grit silicon carbide and 150 grit diamond, cooled with water. The wet saw rotates at 1725 RPM, yielding a face velocity of 6322 surface ft/min. The test samples are 12mm diameter quartz and Pyrex 7740 tubing, standard wall. I made every effort to duplicate the feed rate for each cut; I tried to match the feed rate of that necessary for the silicon carbide wheel, recognizing that it would be somewhat slower than what the diamond could manage. I dressed the wheels before every cut.

Before making the butt seals, I cleaned the samples in an alkali detergent ultrasonic bath for one minute, followed by a hot water and then distilled water rinse. The samples were allowed to air dry. I treated the samples in the micrographs in the same manner.

The micrographs are SEM (Scanning Electron Microscope) images. Without getting into the workings of electron microscopes, let me just add that images were captured using a relatively low (5 kV) acceleration voltage, and that the samples were sputtered with a thin film of gold/palladium to eliminate charging.

Findings: In the interest of comparison, I include only micrographs of the same magnification, in this case, 10,000 X. I hasten to point out, that by themselves, these miniscule perturbations would form bubbles so small that no conventional light microscope could possibly resolve them. These clearly are not the whole cause for the formation of bubbles visible to the naked eye. Rather, these images show the different effects the two abrasives have on the surface of the glass itself, which leads to the formation of bubbles.

Photos 1 and 2 show the effects of the 150 grit diamond wheel. Photo 1 is the quartz sample, photo 2 is the Pyrex. It is important to notice the similarity of the two surfaces.

Photo 1. Quartz - 150 Diamond

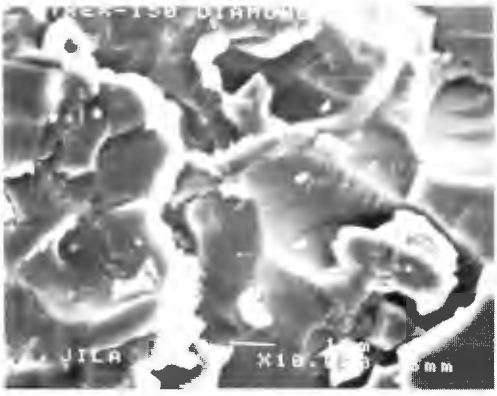

Photo 2. Pyrex - 150 Diamond

Fractured features are clearly evident in both the quartz and Pyrex. Characteristic Wallner lines and hackle marks are evident in both samples. In fact, there is nothing here which distinguishes the two from one another. The diamond, being very much harder than either of the glasses, evidently cuts by means of small scale fractures at the interface of the glass and the diamond particles. These micrographs bear out the assertion that glasses belong to a category of materials that "undergo predominantly microbrittle fracture in the process of chip formation in grinding."[1]

The next two photos, showing surfaces left from the 120 grit silicon carbide wheel, are as different from each other as they are from the first two. Photo 3, the quartz, displays much smaller surface features than photo 1. However, close examination still reveals a fractured surface. The Pyrex in photo 4 appears "smeared," perhaps fused at its surface. The speculation here is that the silicon carbide, being not nearly as hard as the diamond, generates enough friction at the interface to melt the glass. The quartz, having a much higher melting range, still must fracture at the interface.

Hardness is a measure of the ability of the surface molecules or atoms to resist being pushed aside or otherwise displaced. Without getting into the intricacies of the various methods of hardness testing, I will use this space to describe the one most commonly used in this country for glasses, ceramics and abrasives. It falls under the general

Photo 3. Quartz - 120 Silicon Carbide

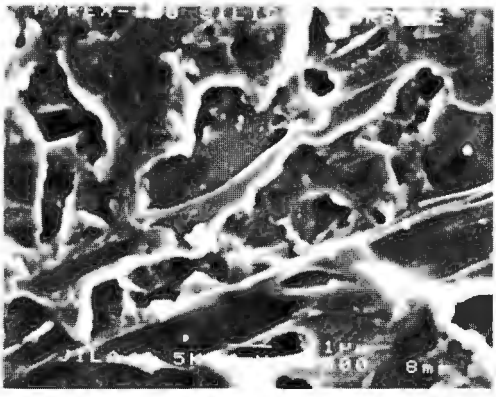

Photo 4. Pyrex - 120 Silicon Carbide

category of microhardness testing, and is known as Knoop Hardness (HK), named for the inventor of the characteristic indenter. The Knoop indenter is a diamond faceted in pyramidal form in such a way as to leave a diamond shaped indentation in the test material such that one axis of the diamond is longer than the other, the approximate ratio being 7:1. The hardness number (HK) is the ratio of the load applied to the indenter to the unrecovered projected area of indentation.[2] Simply put, the number varies with either the change of force applied, or hardness of the material tested. On this scale, Pyrex has a hardness of 500, quartz 800-1000, silicon carbide 2000-3000, and diamond 7000-10000 HK.

There is another difference in the properties of these two abrasives which should not be ignored. The thermal conductivity of diamond is 50 times better than silicon carbide, diamond being around 2100 (W/m x K) to silicon carbide's 42 (W/m x K). This means that the diamond carries away the heat generated in the grinding process much better than the silicon carbide, further contributing to efficient microfracture chip formation.

Photo 5 is the image of a surface starting out similar to photo 4, but subsequently etched in 50% HF for 90 seconds.

Observations in the glass shop show that only photo 4 represents a surface sure to form

Photo 5. Pyrex - Silicon Carbide Etched

a line of bubbles when fire polished and sealed. It is the only surface which appears to have undergone thermal effects, in this case, melting. This is the major difference apparent in these micrographs. What might also occur during the interaction of the glass with the silicon carbide wheel in this severe process is the incorporation into the glass itself of some impurity present in the wheel, either as abrasive or as binder. It may become trapped behind the fused surface, the ultrasonic cavitation unable to liberate it, or become a component of the glass chemistry itself, reacting poorly upon reheat.

Conclusions: In some ways this investigation gives rise to more questions than it answers. While we can see here an obvious connection to bubble formation with a distinctive surface, it only goes part way toward explaining why. If this were the whole explanation, then why do our tungsten carbide glass knives, when we ply them to Pyrex in a process which seems much less severe, form bubbles in the same manner? Do we in fact, generate as much heat at the interface because the pressure transferred to the surface of the glass, reduced to a knife edge, translates to heat? Why do the side ring seals for double and triple walled vessels, having been ground free hand with a silicon carbide belt on a wet sander, not form bubbles?

It occurs to me that we, as glassblowers, know much about glass from experience and observation. While this is valuable knowledge won in legitimate fashion, new methods of investigation, such as electron and atomic force microscopy, available to us only recently, can deepen our understanding of the materials we work. The more we understand about glass, the better able we will be to expand its uses and demand. There is much investigation to be done in this area. This represents only a scratch on the surface, as it were.

Notes:
1. E. Ratterman and R. Cassidy, "Abrasives," Ceramics and Glasses, ed. Samuel J. Schneider, Jr., Engineered Materials Handbook, vol. 4 (Materials Park, OH: 1991) 329.
2. The formula is: $HK=P/A=P/Cl^2$, where P is the load applied in kilograms; A is the unrecovered projected area in mm^2; l is the measured length of the long diagonal in millimeters; and C is 0.07028, a constant of the indenter relating to the square of the length of the long diagonal.

Making a Low Temperature Dehydrogenation Reaction Cell with Zeolite 13X Polyethylacrylate Separation Membranes

by
William J. Wilt
Chemistry Department
CAS Technical Services
State University of New York at Albany
Albany, New York 12222

Abstract

This paper will discuss the design of a leak proof experimental glass apparatus used in the attempt of obtaining (trace) amounts of Benzene by way of a flow of Cyclohexane through non-glass (Zeolite) membranes. Although, a few comments will begin with a fuller explanation of this experiment and possible implications for everyday life, the main focus will be on how such an apparatus, namely one with highly flammable vapors passing through a membrane, was arrived at using readily available glass catalog components.

Introduction

Recently a researcher in the Physical Chemistry Department asked me to make a simple project. It was a somewhat small glass cell, approximately 1 1/4" in diameter by 4-6 inches tall. This cell or apparatus was to be filled in the bottom with a certain small amount of the solvent Cyclohexane, then slowly heated via an oil bath. The resulting Cyclohexane (CH) fumes were to penetrate and flow up through a specially prepared membrane called Zeolite 13X Polyethylacrylate. These passed-through vapors were then to be distilled (under a vacuum of 2mg Hg), condensed via a series of traps, and the collected results would contain a small amount of the chemical Benzene. The chemical formula for this experiment would then be as follows: $C_6 H_{12}$ Cyclohexane $\rightarrow C_6 H_6$ Benzene. The chemicals are commonly represented in Diagrams 1-4.

On the shorthand version (i.e. stop sign pictures), note particularly the circle inside the Benzene diagram. This circle represents so-called "double bonds." These bonds allow for easy attachment and forming of countless other compounds.[1]

Low Temperature Dehydrogenation Reaction Separation Membranes

Previous attempts to make Benzene from Zeolite membranes had been successful, but none at a specific low temperature of the Cyclohexane as in this experiment.[2] Certain additives, namely Titanium and Nickel were added to the Zeolite membrane, also a certain chemical called Polyethylacrylate. This resulted in what is termed in Physical Chemistry a perfect separation of two compounds.[3] So as not to confuse the reader, I want to note one other important matter. The focus of this experiment was not to *invent per se* new ways of *producing Benzene*. Benzene is indeed already made available from crude oil distillation in mass quantities; the method of doing this is typically by using those tall fractional distilling columns very commonly observed along parts of the New Jersey Turnpike and certain roads in California (see pictures 1 and 2). Rather, the intent

CYCLOHEXANE

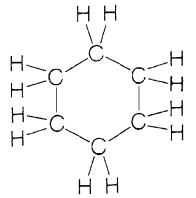

Diagram 1

BENZENE

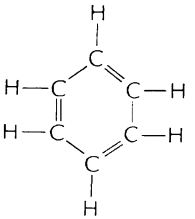

Diagram 2

CYCLOHEXANE

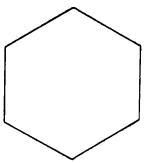

Diagram 3

BENZENE

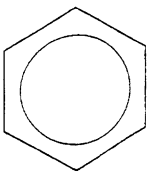

Diagram 4

of this project was to show that Benzene *could be made* from Cyclohexane with these specially treated Zeolite membranes, and again at a much lower temperature, 70-90 C (boiling point of CH is 81 C). These membranes were treated with Polyethylacrylate, which is very toxic and strong in odor; subsequently gloves and hoods had to be used at all times.

As the treated membranes were respectively placed above the Cyclohexane, the Cyclohexane fumes were heated and the fumes rose and passed up through the membranes. During this process, the hydrogen atoms from the Cyclohexane were essentially stripped away, resulting in a new molecule, namely Benzene. This process of removing hydrogen is known typically as Dehydrogenation. Dehydrogenation, as in the title of this paper, is actually quite familiar to us: that term is used to describe how saturated fats (butter, lard) are changed into unsaturated ones (canola[4], olive oil). Having said all of this, one must stop and ask the simple question: what relevance does this very unique and specialized experiment actually have for us in our everyday lives? The answer for this lies in what is called in physical chemistry the process of pure separation. From similar separation projects, interesting new compounds, notably those in the pharmaceutical industry, can be made, i.e. new medicines. Before I begin talking about how I made the apparatus, I do want to mention a few things about the chemical Benzene. Benzene in more recent times has, regretfully perhaps, been known only for its dark or negative side. Indeed, since Benzene was recently identified as 1 of 20 known carcinogens in the world, a common can of it which, 30 to 40 years ago used to be on one's garage shelf, is now rarely to be found.[5] In gasoline, however, Benzene plays a very important and critical role. Yet, because of its carcinogenic features, it is now, at least in North America not the rest of the world, very strictly regulated and is only a very small part (0.1 to 4.4%) of gasoline.[6] Nonetheless, Benzene is what one so easily identifies by smelling it at the gas pump. For this reason, we now have big round rubber collars on the

handles that most of us rarely notice.[7] In total contrast to these negative effects of Benzene, it is quite necessary to us. Indeed, an entire array of common everyday products would be impossible without it. To mention just a few: plastics, polyurethane foam, agricultural treatments, aspirin and even in research certain new medicines for blood disorders.[8]

Now, the apparatus itself. As already alluded to, the whole focus of this experiment revolved around the membranes called Zeolite 13x Polyethylacrylate. The sample first given to me was very specific in terms of a precise 25mm diameter (see picture 3). It was

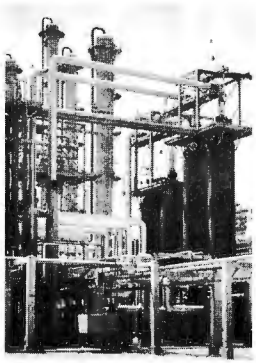

Picture 1

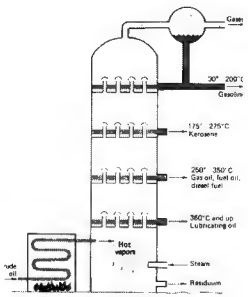

Picture 2

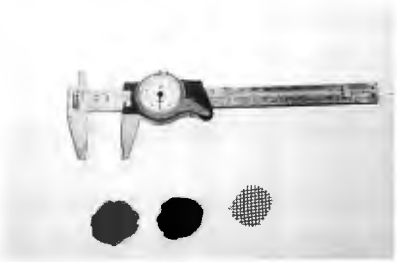

Picture 3

fairly pliable and looked very much like kids' Play Dough, although it was a very dark gray color. I was asked to design and manufacture a glass apparatus capable of holding the 25mm membrane inside. The bottom 25mm od section of the glass apparatus was to be filled with about 0-30ml of Cyclohexane. After this, the Cyclohexane would again slowly be heated from the outside (via an oil bath) and rising fumes were simply to pass up through the membrane. The gases passed through the membranes under constant steady vacuum (2mg Hg) would finally be distilled and trapped. The samples were then to be taken to an NMR for respective analysis of Benzene. The problems making this piece were fourfold:

1. To make an apparatus to match exactly these precisely sized membranes of 25mm od
2. There was an obvious leakage problem of the Cyclohexane fumes around the membrane (CH being very flammable)

3. To maintain a constant leak-free vacuum
4. To provide easy disassembly for inserting and removing these membranes

My first thought was to simply take a glass fitted tube and place the membrane inside it. This idea was quickly discarded since first there were no tubes available to fit the exact diameter of these membranes. And much more importantly, there was the problem of how to hold them only by their edges and to have little to nothing actually touching between the membrane and the rising CH fumes. The research student was aware of this but still insisted on my making certain custom-made glass flat flanges to hold the membrane exactly in place. This worked relatively well for the first few trials, but, as other membranes were inserted and removed, invariably the glass flat flanges would be easily broken, mostly from overtightening of the outside metal clamp. A more acute problem was that as pressure would build up from the heated Cyclohexane, these membranes would "puff up" as it were and would be drawn up and out of the flat glass flange holders. Several other options were tried using o-ring joints, ball joints and even ball joints with o-rings on them. Yet, they all only resulted in improper fits and leakage for what was now this problem membrane. More recently, I was asked by a different set of researchers to retry this project using normal glass joints somewhere in the apparatus for easy disassembly. A joint size 45/50 was chosen. It was at this point, while thumbing through a glass catalog, that I finally arrived at the solution. It was to use a straight drip tip joint, (note: not cut on an angle) to hold down this membrane. (See picture 4, diagram 5). This accomplished three things:

1. The membrane was held down only by its outer edges, thus giving a good unobstructed flow of CH
2. By using joints, it was leak proof
3. It had easy disassembly

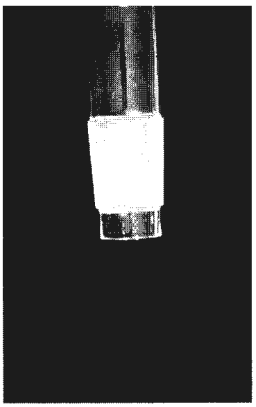

Picture 4

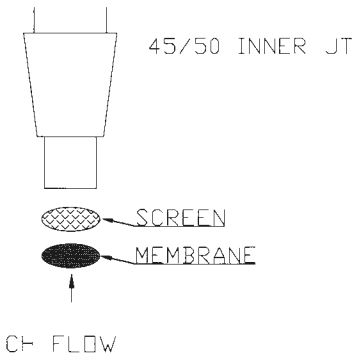

DIAGRAM 5

A small matching metal screen was placed on top of the membrane to avoid the "puffing up" problem. Then the straight drip joint was inserted and slightly modified in terms of its length, to ensure a proper tight fit on the membrane and screen as the joints were put together. Lastly, I also added a set of hooks and springs on the outside of the joints to avoid any opening up of these joints during operation. In the end, this technique worked fine, and currently this apparatus is still used without any incidents during daily operation (See pictures 5, 6, and 7).

Picture 5

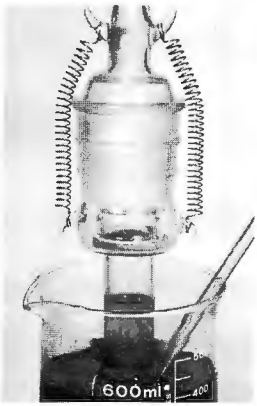

Picture 6

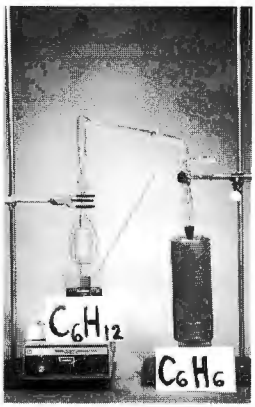

Picture 7

Conclusion

I conclude with an open acknowledgement as to whether any other glassblower would be ever asked to make this exact same apparatus. Nonetheless, there are a few principles that I learned, or rather relearned, from making this project which I believe could help us all in our daily jobs:

1. Glass Catalogs: before beginning any project, one should first look through glass catalogs for possible alternative parts, such as the uncut drip tip joints. I emphasize this as I have found or negotiated for parts and sometimes an entire apparatus at amazingly low prices.
2. To remember that oftentimes what the researcher gives us as a request or drawing and what the glassblower is actually able to make and have function well are two different things.
3. A corollary to this is the advice of a highly-experienced colleague of mine, Adolf Gunther from Advanced Glass Technology: we need to take the necessary time before we begin a job to make our own sketches and outline steps of assembly. With many standard jobs we obviously do not need to do this. I mention this as oftentimes in our hectic work schedule moving quickly from job to job, we only find in retrospect better and more effective ways we could have done something. If we do not rush into them, this will not happen.
4. A journal. Admittedly, a journal is the last thing a glassblower wants to think about after a long hard day of work. Yet I have found it quite helpful to sit down the following morning before the workday begins and make some sort of notation or reminder on a job (sometimes even just on the sketches themselves) before I file it away and begin another.

To conclude, this job was not an extremely complex one, i.e. one with multiple seals, jacketed sections and bends. Yet I hope that this paper will mostly be remembered for the "reminders" I offered at the end: that is, to first go through glass catalogs, to make sketches prior to assembly, and to keep some sort of journal or minimally to attach a notation to a job before beginning new ones. I have found these minor hints to be of invaluable help as we glassblowers confront the increasingly more specialized jobs that come to us everyday.

Acknowledgments: I would like to thank Dr. Harry Frisch, Professor of Physical Chemistry at the University at Albany, his research staff Haoran Deng-Nemer, Wanxue Zeng and Ms. Lei Wuang, and Adolf Gunther of Advanced Glass Technology. Thanks also to my supervisor Charles Heller for kindly providing for me a computer in order to research at home information for this and other papers.

Notes

1. T.R. Dickinson, Understanding Chemistry: From Atoms to Attitudes (New York, NY: John Wiley & Sons, 1974) 250.
2. Harry L. Frisch, "Low temperature dehydrogenation reaction-separation membranes using Zeolite 13x polyethylacrylate, *Journal of Membrane Science* 988 (1998).
3. *Ibid*
4. Dickinson 238, 265.
5. "Carcinogenic properties benzene." Online. Internet. 1 June 1999. Available http://www.angelfire.com/me/a/abaddon2/toxicity.html
6. *Ibid*
7. "Why your gas pump has a collar," NIEHS journal supplemental details benzene toxicity. Online. Internet. 1 June 1999. Available http://jeeves.nih.gov/oc/news/benzene.htm
8. "That useful molecule called benzene." Online. Internet. 1 June 1999. Available: http://www.angelfire.com/me/abaddon2, or Schmidt@golden.net

Suggestion: go to www.lycos.com for more updated information on benzene, also www.webmolecules.com for 3D images Benzene, Cyclohexane (VTML required).

An Observation of Devitrified and Phase Separated Glass with an AFM

by
Gary Coyne, Eva Huang, and Feimeng Zhou, Ph.D.
Chemistry Department
California State University, Los Angeles, California 90032

When I first saw pictures of the molecular structure of mica at the atomic level (see Figure 1), my first thought was "Could one see glass molecules frozen at the moment of strain?" My route toward this objective has been unsuccessful to date, but other opportunities have led to some very interesting observations and discoveries of glass surface phenomenon of both devitrification and phase separation of borosilicate glass.

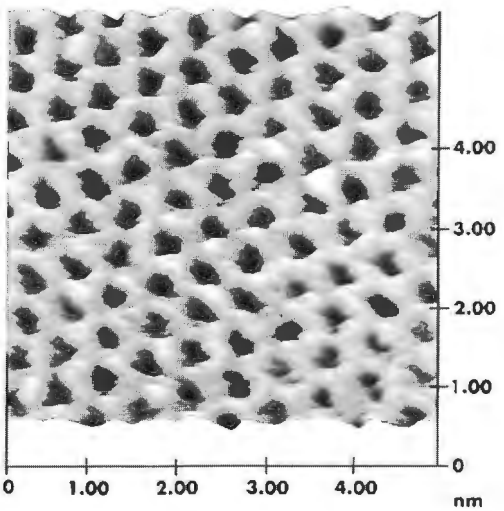

Figure 1. A 5x5nm View of Mica at the Atomic Level.

Introduction

The ability to see beyond the levels of an optical microscope has been a long sought dream for researchers. Although showing worlds never before seen with the unaided eye, the light microscope was limited to about 2000 times. This was limited to the wave length of light, at about 4000 Ångstroms. The electron microscope, developed in the 1930s, brought magnification of up to one million times due to the smaller wave length of the electron, about 0.5 Ångstrom.[1] Then, in 1981, the Scanning Tunneling Microscope (STM) achieved magnification in the range of 100,000,000 times. With the right conditions and materials, resolution can reach 1 Ångstrom. (To get a perspective of how big (or small) an Ångstrom is, see Figure 2.)

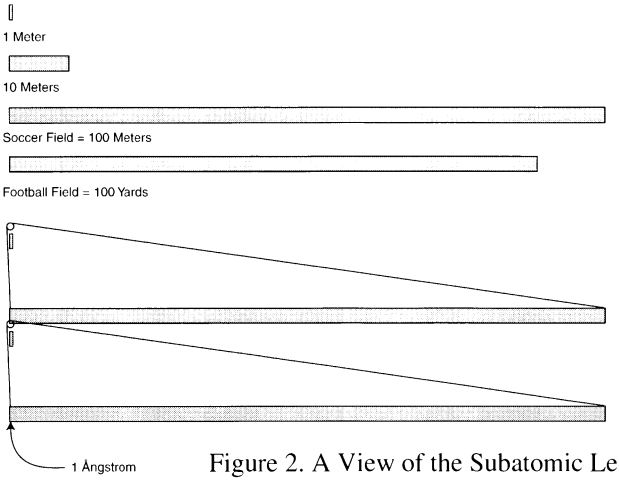

Figure 2. A View of the Subatomic Level

One millimeter (mm) is 10^{-3} meters
One nanometer (nm) is 10^{-9} meters
One Ångstrom (Å) is 10^{-10} meters
The ratio difference between 1 millimeter and 1 meter is 10^{-3}
The ratio difference between 1 meter and 100 meters is 10^{-2}
The ratio difference between 1mm and 100 meters is 10^{-5}

If one millimeter was the size of a soccer field, and you took one of its millimeters and made it into the size of a soccer field, then the size of one of its millimeters would be the size of an Angstrom.

Scanning Tunneling Microscopes function by attaching the desired object to the STM and placing the STM in a vacuum chamber. Then, the micro-tip of the STM is placed extremely close to the object after which a small current is applied to the object and the micro-tip. As the tip scans along an "x" and "y" grid of the sample, a voltage "tunnels" across the gap between the sample and the tip. The tip raises up and down (the "z" access) to maintain the same voltage. Thus the topography can be determined, and for the first time a full three- dimensional viewing of a micro-object can be created.

Unfortunately, there were obvious limitations to STM: (1) the object had to be small enough to fit into the device, (2) the object had to go into a vacuum chamber, and (3) the object had to be able to conduct electricity. Although one can lay a very thin metallic film on the sample to obtain the needed electrical conductivity, this last limitation essentially prevented, or limited the observation of all biological and other non-conductive materials, such as glass.

Then, in 1986, the Atomic Force Microscope (AFM) was invented which bypassed the limitations of the STM. In basic "contact mode," the AFM drags a probe along an "x" and "y" route along the sample surface. The force of contact is in the range of intermolecular forces, ergo the term "atomic force." (This paper is concerning itself only with what is called "contact mode" on the AFM. Not used or discussed is the MAC (Magnetic Alternating Current) mode, friction mode, conductivity mode, and many other techniques of AFM that utilize various physical properties and/or principles of particles at the atomic level.)

Basic principle of Atomic Force Microscopy operation.

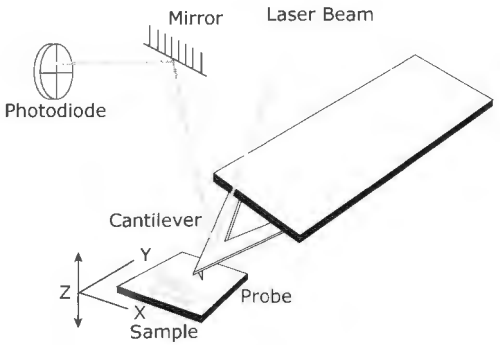

Figure 3.

In regular operation (see Figure 3) the probe tip is supported on a cantilever which is in turn attached to a structural block. Once the probe makes contact with the sample, it must be adjusted to counter the effects of the Van der Waals forces, or rather the inherent molecular adhesive forces between two objects, in this case it is the tip and the sample.

These forces must be accounted for for each sample, and occasionally for each change in imaging resolution. A laser is then directed at the end of the cantilever and this is reflected against a mirror and in turn against a photodiode. The relative position changes of the laser on a photodiode are interpreted as the deflection of the cantilever and can be accurately translated into a vertical distance measurement.

As seen in the top of Figure 4, the type of tip used on the Molecular Imaging probe is Si_3N_4 and is placed at the tip of the cantilever, and the base of its pyramid shape is around 5μm. The bottom picture shows a close-up of the tip.

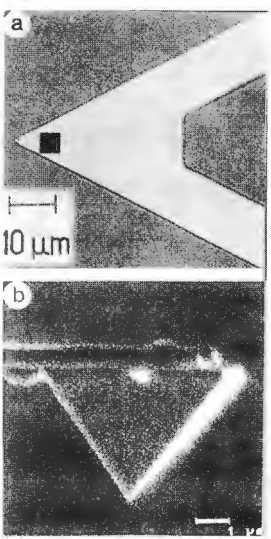

Figure 4.

The ability of AFM to achieve resolution to the atomic level is actually not beyond reason. Some tips are manufactured with a calculated point of one atom, and it simply is an issue of having it drag sufficiently lightly across the surface without doing damage to either the surface or the tip. Other, wider tips can also achieve atomic surface resolution similar in concept to a bowling ball dragging over a surface of marbles. The resolution may not be as great, but the general contours and boundaries of the surface can be determined. The tips used by Molecular Imaging are of the wider, not as pointed, type of tip.

The Procedure

A series of glass samples were prepared using 80mm tubing. The tubing was cut into a small ring and this in turn was cut into small squares so the overall curvature would be as minimal as possible. The glass was then heated by a torch so that the strain was approximately in the middle of the sample.

The sample is then placed in the microscope (See Figure 5) on a metallic disk with double- sided tape. The metallic disk is then stuck to three magnetic rods from below the main body of the microscope. This is more easily seen in Figure 6. Although all three magnetic rods can be rotated in the "z" axis by hand, only one can be controlled by the computer attached to the system. Normally one places the sample as close as one can on a visual basis, and then the computer "approaches" the sample until contact is made by the probe. The irregular surface of the glass made the visual alignment somewhat difficult.

Figure 5

The final approach with the tip is not done until the microscope is placed in a vibration free environment. The box that was used for this work is shown in Figure 7. It is simply a wooden box with insulating foam on all sides of the microscope and the microscope itself suspended by some bungee cords. Standing with the instrument is one of my co-authors, Eva Huang.

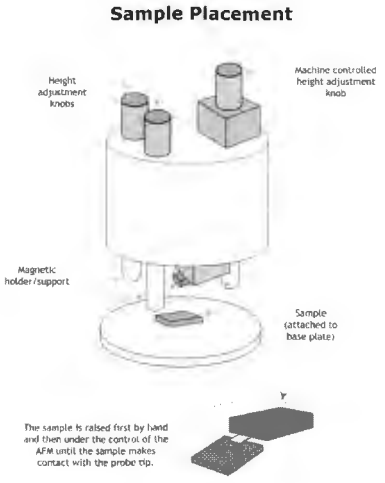

Figure 6.

Figure 7. Eva Huang and the Microscope.

Once contact is made, the amount of force of the probe tip against the sample must be set. As stated, there are Van der Waals forces pulling the tip against the surface of the sample. What the user must do is apply a sufficient amount of pressure in tandem to the Van der Waals force to achieve a proper force for a reading. If this force is too great or too small, the tip "crashes" meaning that the AFM cannot interpret the readings from the tip. A greater concern is if the pressure on the sample by the tip is too great causing the cantilever to break.

The Results (part 1)

The greatest resolution I was able to achieve was a view of 1200 nm X 1200 nm; this is seen in Figure 8. This is a far cry from the 10 nm X 20 nm range that was necessary for my goal observation. This was in part due to my inexperience with AFM and this

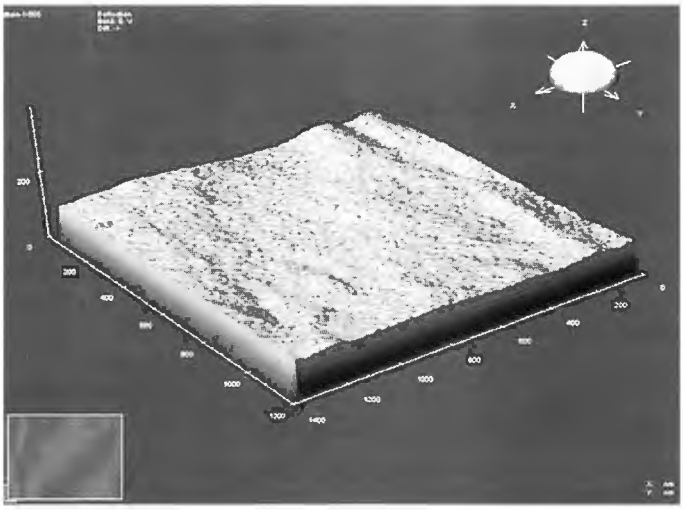

Figure 8. Flame Polished Glass 1200 x 1200nm.

equipment in particular. The probe tips of this AFM have a radius in the range of 50-75Å. This is considered far too big to detail a non-repeating structure like glass.

One of the initial problems in my goal was caused by some miscommunication with one of the employees of Molecular Imaging, the company that manufactured the AFM being used. They had many times created images of crystals at the molecular level. Unfortunately, they were under the impression that glass was a crystal. It is relatively easy to get molecular images of crystals because the repeating patterns created by the atoms can be assisted by the computer. In later conversations, when it was commented that glass was not a crystal, their expressions changed and they said it was not possible on their equipment. There have been articles that described the production of annealed glass ($Ge_{20}Te_{80}$) images at a resolution of 20 x 20 nm.[2] I hope one day to achieve resolutions at this range.

The Results (part 2)

Having been stymied in my original goal, I took advantage of my AFM access for a secondary interest: an observation of devitrified glass.

A sample of devitrified glass was easily created by heating the center of one of the glass samples (from the earlier test) until soft. After removing the glass from the flame, and just before it became too hard, a gentle compression of the softened area created the desired devitrification.

As seen in Figure 9, the image of devitrification is much more textured than the fire-polished glass surface. The resolution of this picture is 10,000 X 10,000 nm, or 0.1mm of the mm inside our magnified mm soccer field. Please note that AFM shows vertical resolution in a 2D view by a change in color. Here, the lighter the color, the taller the material. It is easy to interpret this image as gentle rolling furrows, but rather this image shows a slow rise in elevations (from the top right to the bottom left) with a steep drop off. In other words, the dark is not shadow, but a lower elevation

.

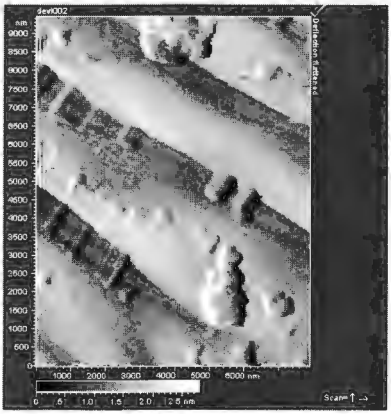

Figure 9. Devitrification at 10,000 x 10,000 nm.

Figure 10 shows a close up of the primary objects seen in Figure 9. A more complete understanding of its shape and contours is best shown with the 3D view of Figure 10 seen in Figure 11. What appears to be a crystal outgrowth proves to have a crater-shaped contour. What is interesting is that the left side of each "crater" has a lifted side which drops in elevation to the right side. Outgrowth or crater, what is being observed is a crystalization process. This is an excellent view of phase separation.

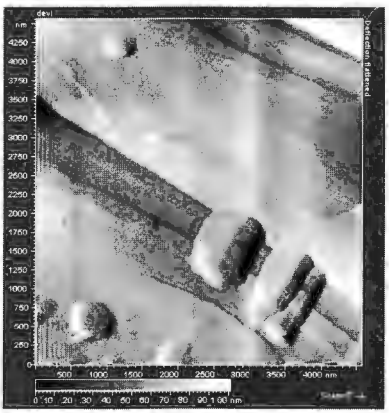

Figure 10. Devitrification at 4500 x 4500 nm.

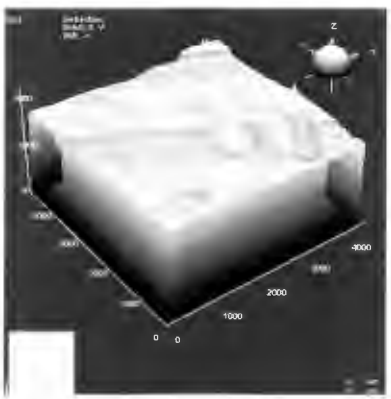

Figure 11. Devitrification 4500 x 4500 nm, 3D.

Phase separation commonly occurs when glass is kept at too high a temperature for too long. This is why it is not recommended for glass to be kept at the annealing temperature for over two collective hours.[3] An explanation of phase separation is that some atoms such as silica bonds more easily to oxygen than other oxides. Likewise, the bonds of sodium, lithium, or potasium are weak compared to calcium.[4] Thus, in the raised temperature of an annealing oven, the extra oxygen atoms will link to the silica atoms forming a tetrahedra and sodium, lithium, and potasium are likely to give their oxygens up to the calcium. If a sufficient number of calcium atoms are in proximity to each other, a crystal will form within an otherwise homogenous mixture of glass.

To better observe phase separation caused by prolonged exposure to high heat, I happened to have the glass tube in my oven that has been used to attach dewars to my vacuum line. It has been in the oven for countless annealing operations for over seven years. The tube was removed and samples of the inside and outside surfaces of the tube were prepared for observation at the AFM.

Figure 12 shows the outside surface of a phase separated glass at 7500 X 7500 nm. This is noticeably unlike the smooth surface seen in Figure 8. One of the obvious features seen are the "bead" like particles scattered across the surface. It is unknown whether they are a surface phenomenon of some kind or a deposition of some material from within the oven. The oven used is a standard Wilt oven. Among the materials that could be represented here include brick dust (with a melting temperature of about 2000°F), the ceramic fiber (with a melting temperature of about 2800°F), spalling from the nickel that is in the heating elements, and finally the mortar or cement holding the bricks in the oven.[5] On the other hand, it may not be a deposition at all, but rather a beading up of phase separation materials on the surface of the glass.

The area of Figure 12 in 3D is seen in Figure 13, a 2100 X 2100 nm view showing the beads projecting up about 250 nm. It also shows a series of troughs, or "scratches" running from upper left to lower right.

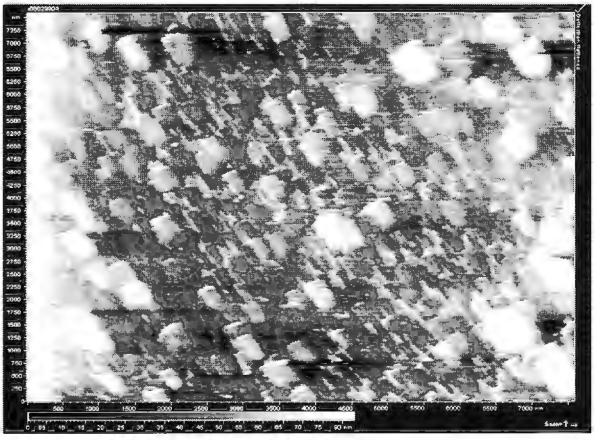

Figure 12. Phase separation outside 7500 x 7500nm.

The inside of the evacuating tube has been in the same high temperature environment for the same time, but in a vacuum. Its surface, as seen in Figure 14, is profoundly different. Although at the same resolution as Figure 12, 7500 X 7500 nm, the large rough surface

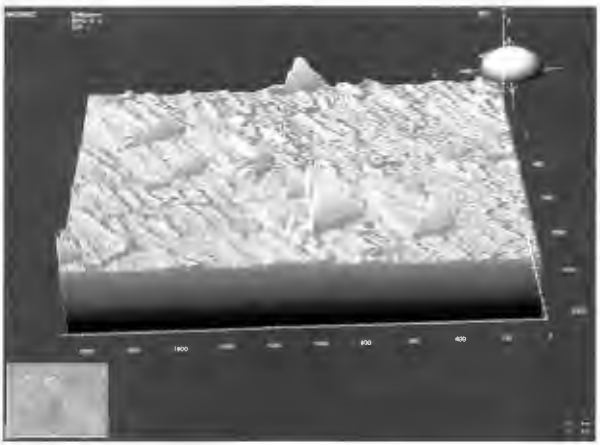

Figure 13. Phase separation outside 3D 2100 x 2100 nm.

is now littered with sharp narrow crests. This is better seen in Figure 15 showing a 3D view at 2900 X 2900 nm. The crests of these growths are also as high as 200-250 nm, but one can truly see the rows of crests that are more difficult to see in the outside view shown in Figure 13.

Conclusion

Like a good mystery, this has created more questions than answers. It is speculated that the crests shown in Figure 15 line up lengthwise along the evacuation tube. This would make sense in that they represent expansion cracks created by the continual expansion and contraction of the glass during the annealing process. Unfortunately, we did not pay attention as to how the glass piece was placed on the mounting plate, so presently the true alignment and their cause is only speculation.

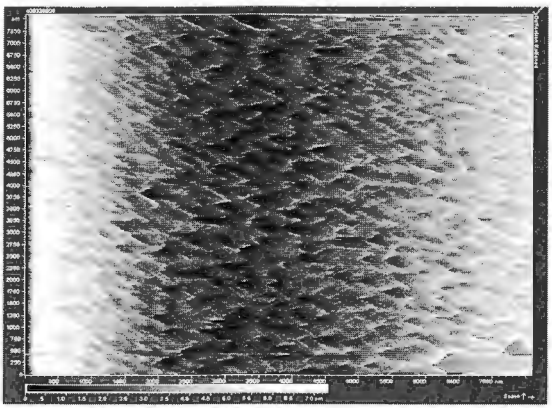

Figure 14. Phase Separation inside 7500 x 7500 nm.

It is unknown at this point in time whether the lack of these features on the exterior are due to the presence of air or whether their great quantities on the inside is due to the vacuum within which the inside surface has been maintained.

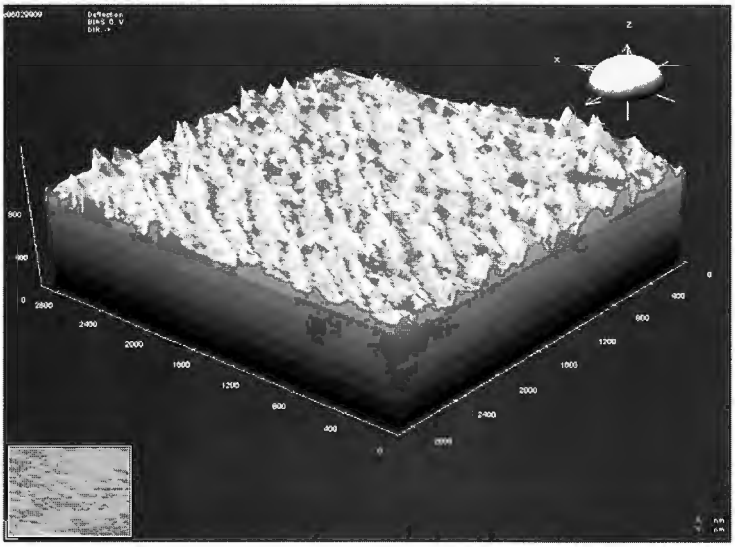

Figure 15. Phase separation inside 3D 2900 x 2900nm.

Acknowledgements

This is not the first research done by a member of the ASGS using AFM: At the 43rd Annual Symposium, Mike Souza examined Aluminosilicate glass and how the surface was radically smoothed after flameworking in his poster entitled "Atomic Force Microscopy Scans of Glass Surfaces used in Polarization Cells." Likewise, Hans Rohner is presenting a technical paper at this Symposium entitled "Investigating Bubble Formation in Butt Seals with the Aid of an Electron Microscope." Clearly, AFM and the study of glass presents many opportunities for further research.

I would like to express my appreciation to Dr. Feimeng Zhou who let me have total access to the AFM, providing he was not using it. I would also like to thank Eva Huang, who created the phase separation images for me and performed most of the computer work for the final images.

End Notes

1."Microscope," *Microsoft® Encarta® 98 Encyclopedia.*© 1993-1997 Microsoft Corporation.

2. K. Ichikawa, "The Nanoscopic Structure of Annealed $Ge_{20}Te_{80}$ Glass: Quasi-Atomic-scale Imaging Using Atomic-force Microscopy," *J. Phys.: condens. Matter* 7 (1995) L135-L139.

3. Annealing instructions, Glass Warehouse

4. L. Holland, The Properties of Glass Surfaces, (New York, NY:1964) 8.

5. Daniel Wilt, personal conversation, June 14, 1999.

Problem Solving Tools for Glass Cracking

by
Robert Sweeney
Osram Sylvania, Inc., Central Research
Beverly, Massachusetts 01915

Glass has unique properties that make it quite different from other solids. However, it must be treated with proper respect or it will fail and crack. Glass strength is related to surface and thermal conditions. Fracture analysis is an important technique for determining the root cause of brittle material failure (i.e. glass & ceramics). The newly-fractured surfaces can reveal important information on where the crack started, why the crack started, the stress conditions in the glass when it cracked and how much force was used to break the glass. This paper will outline the important features of fractures so that one can use this information to determine the root cause of failure. Once the root cause is known, improvements can be made to the process to prevent such failure modes.

A most unique material

Glass is ...

- a non-crystaline brittle material at room temperature
- plastic at above the transformation range
- easily shaped and formed
- prone to damage if not managed properly

[thermally and mechanically]

Why Does Glass Crack ?

Cracks will develop in glass for one or more of the following basic reasons:

- **Stress, 4 types**
  Thermal and/or Mechanical, Temporary and Permanent
- **Surface Defects**
  Foreign materials, scratches, chatter marks
- **Poor Geometry**
  Sharp or reentrant angles, wall variations at seal joints

These conditions create *stress concentrations* that affect strength

Types of Stresses

	Thermal Stress	Mechanical Stress
Temporary	***Heating Cooling***	***Impact Bending Squeezing***
Permanent	***Temperature gradients through the transformation range***	***Glass / Metal Glass / Glass***

Thermal Stress: Temporary (below strain point)

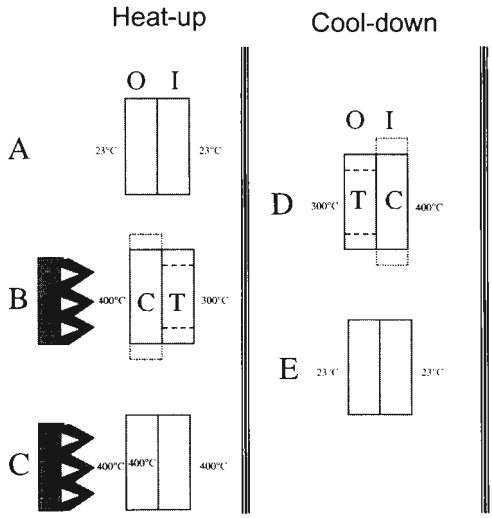

A. Room temperature no stress

B. Outside glass expands with heat. Inside glass (cooler) in tension.

C. Uniform temperature, no stress

D. Outside surface cools first, tension

E. Room temperature glass, no stress.

Thermal Stress: Permanent (above strain point)

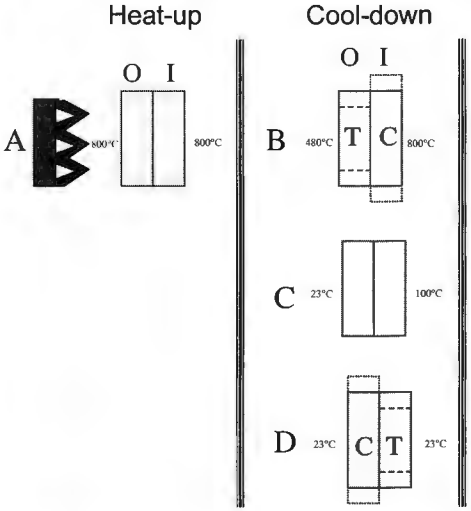

A. Glass heat above the strain range will relieve all stresses

B. Outside glass freezes first, inside still expanded & above the strain range. (size fixed)

C. Outside surface at room temperature
Inside still hot and expanded

D. Inside continues to contract, outside resists creating permanent stress

Thermal Stress

- **Temporary stresses** are produced when heated glass expands faster than the cooler adjacent glass ***below*** the strain point.

- **Permanent Stresses** form in the glass when it is heated ***above*** the strain point and then cooled non-uniformly through the transformation range.

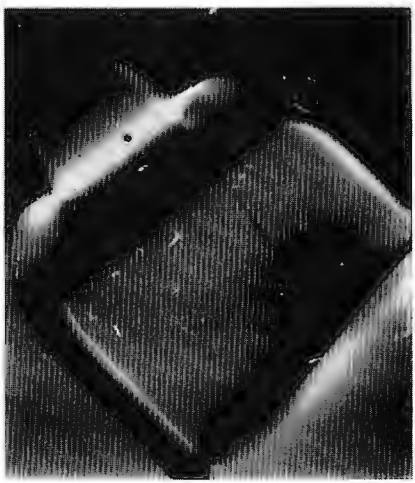

Understanding Viscosity

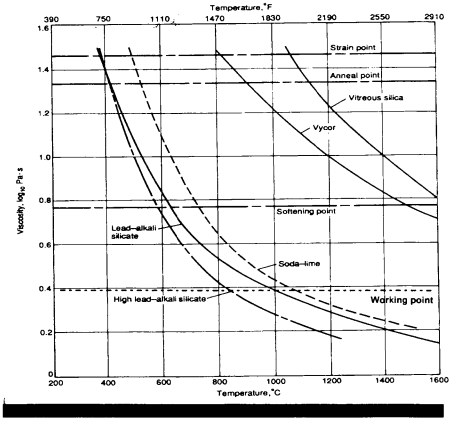

Softening Point

Lead glass = 630°C

Soda-lime = 696°C

Borosilicate = 820°C

Aluminosilicate= 1020°C

Vycor = 1530°C

Fused Silica = 1683°C

Ref. ENGINEERED MATERIALS HANDBOOK Vol.. 4

Understanding Viscosity

	Temperature	Viscosity (Poises)	Remarks
	Room Temperature	10^{22+}	
	Maximum Service Temperature	10^{15+}	Above 10^{15}, the glass is rigid and brittle.
Annealing Range	Strain Point	$10^{14.5}$	The viscosity point at which the internal stress is substantially relieved in 4 hrs
	Transformation Point	$10^{13.3}$	The viscosity point below which glass is plastic, above which glass is elastic.
	Annealing Point	$10^{13.0}$	The viscosity point at which the internal stress in glass is substanially relieved in 15 min.
Working Range	Softening Point	$10^{7.6}$	The viscosity point at which glass will deform under its own weight and begin to tack to other bodies
	Working Point	$10^{4.0}$	The viscosity point at which the glass is soft enough for hot working and forming.

Mechanical Stress: Temporary

Only while the force is present.

Impact - ***force exceeds glass strength***

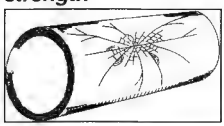

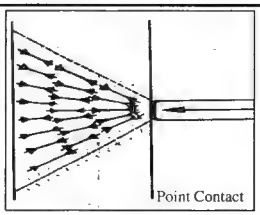

Bending - ***A mechanical bending moment will cause a "cantilever curl"***

Side View

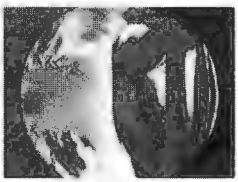

End View

Mechanical Stress: Permanent

Expansion mismatch of Materials

Glass/Metal Seals

Dumet Wire

Glass/Glass Seals

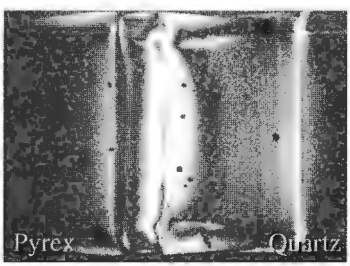

Surface Defects: form Stress Risers

Foreign materials and Bruise Checks *from processing and handling*

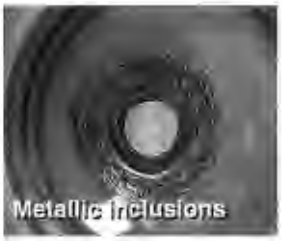

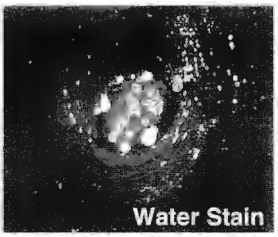

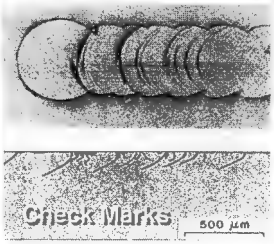

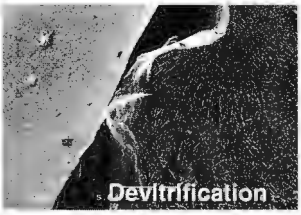

Improper Shape or Geometry

- The leading cause of glass shrinkage.
- Improper glass seals form a sharp angle inward towards the bulk.
- Abrupt glass wall transitions

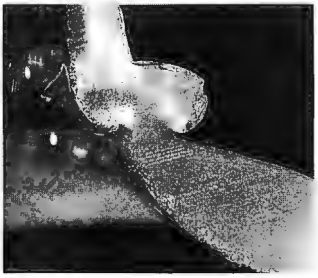

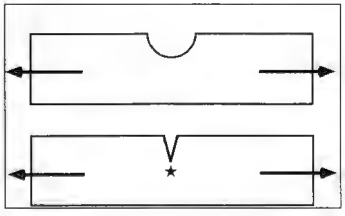

Stress risers make the glass mechanically weak (wall variations and reentrant angles)

Stress Concentrations

Calculating the Effect on Stress Risers

X = S(1+2L/a)

Where X = stress at flaw tip
S = stress on glass surface
L = depth of crack
a = 1/2 width of the flaw

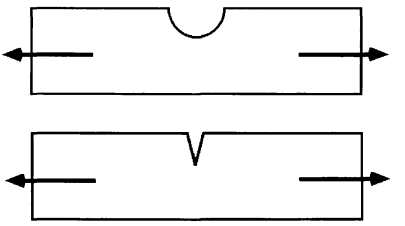

If a piece of glass had a 0.1mm deep flaw, 5um wide, and the stress on the surface of the glass was 1500 psi tension, the resulting stress at the tip of the flaw would be:

$$X = 1{,}500(1+2 \times 10^{-4}\ m / 2.5 \times 10^{-6}\ m)$$

X = 121,500 psi

Tools for problem solving

- **Polariscopes are used for viewing the effect of permanent stress on transparent objects.**

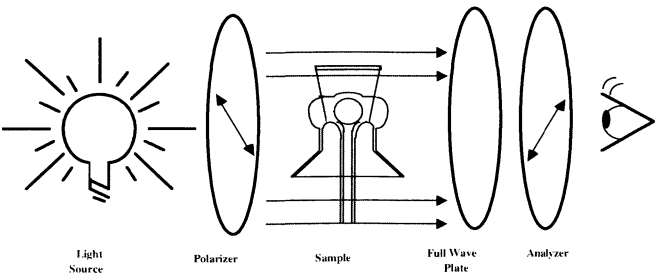

The light source is polarized so that it vibrates in one direction. As this light passes through the sample it will display the stress intensities in blue or yellow color depending on sample orientation. A magenta color will be present if the sample has no stress.

Polariscopes

Immersion Oil

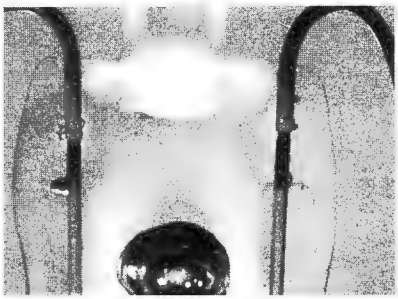

without Immersion Oil

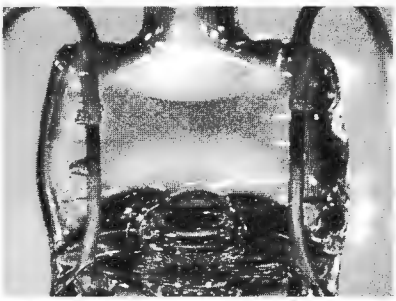

Permanent Stress: Uncontrolled Cooling

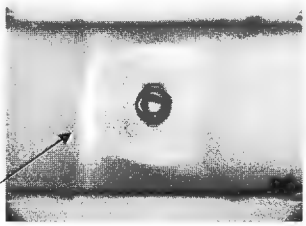

Transformation Range

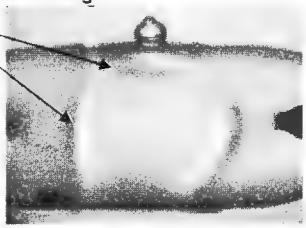

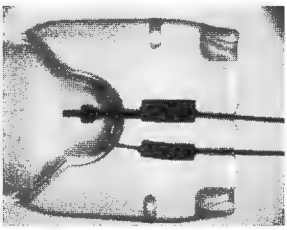

Top View

Mismatch Stress: Fused Quartz/Moly Foil

Side View

Fracture Analysis

- Where the crack started
- What was happening during fracture
- Why the crack started
- How to prevent future fractures

Fracture Analysis: What happened

- When glass breaks, it creates new surfaces that leave particular physical features that remain on the new surface as the crack front travels away from the fracture origin.

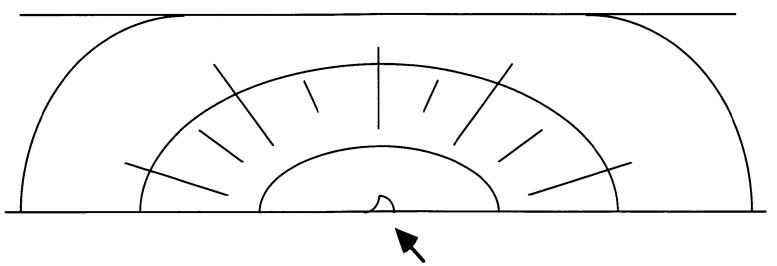

- These features resemble a stone that is dropped into the water

Fracture Analysis: Features

- Wallner lines resemble rib-shaped marks which are perpendicular to the path of the fracture.
- Wallner lines are concave towards the crack origin.

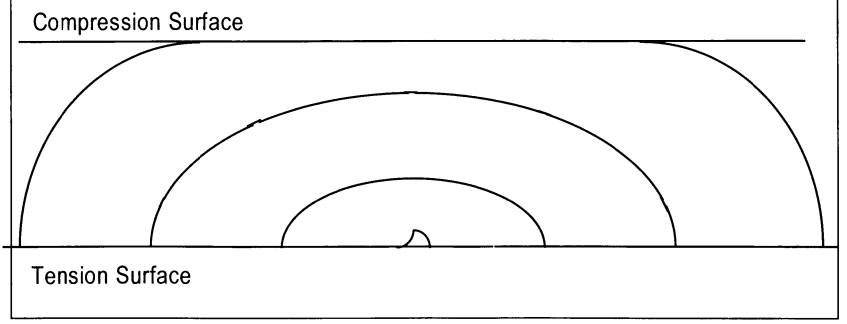

Fracture Analysis: Features

- Hackle marks are splash-like marks that run parallel to the crack propagation.
- Hackle marks form on the compressive side of the glass.

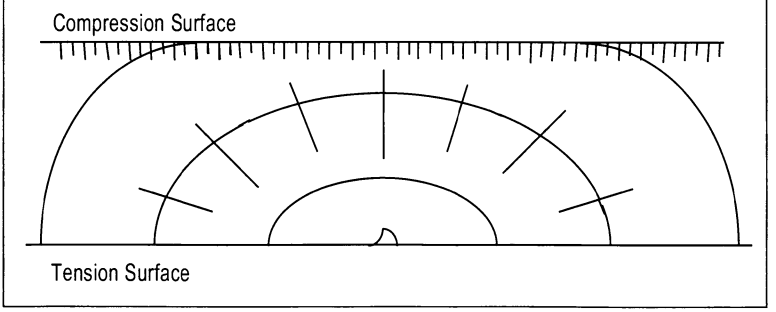

Fracture Analysis: High Magnification is Important

- Crack origin due to metallic scratch on the outside surface.

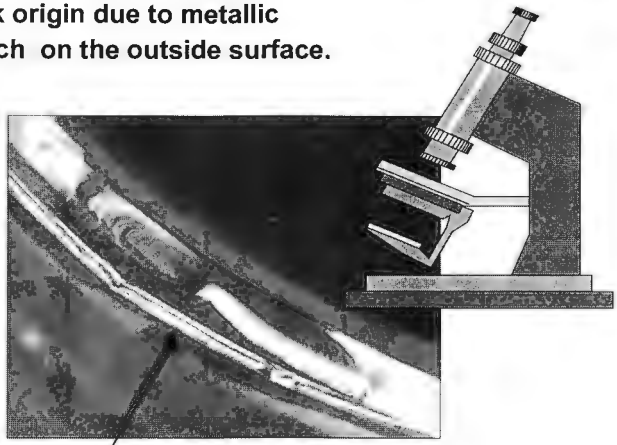

Origin

Fracture Analysis: Glass only breaks in Tension

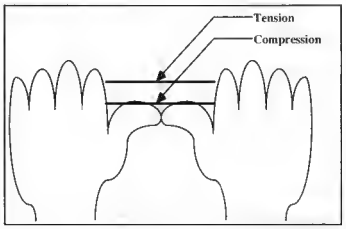

A mechanical bending moment will cause a "cantilever curl"

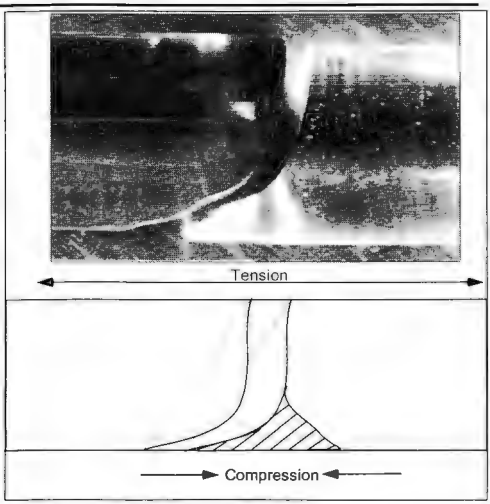

Fracture Analysis: Features

- Mirror Surface **Large mirror plane = Low magnitude tensile stress**
  Small mirror plane = High magnitude tensile stress

Low Force 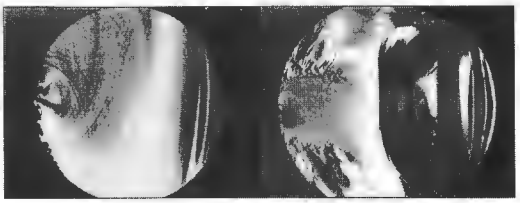 High Force

- Mist Hackle **Surface roughness begins as terminal velocity is reached causing non-coplanar bifurcation.**

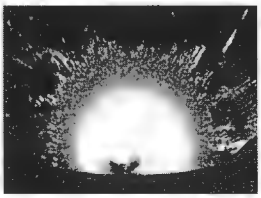

Fracture Analysis: Features

Wake Hackle forms as the crack front moves around the inclusion and reunites as one crack plane.

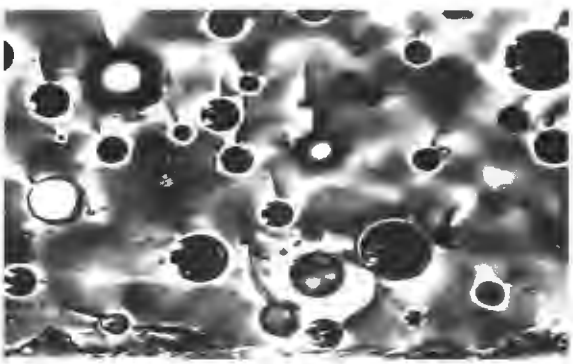

Crack origin ↑

Fracture Analysis

Thermal Fracture due to *central heating* of a disc

Central heating causes hoop tension on the rim

(no cantilever curl)

Fracture Analysis: Draw your Conclusions

- **Timing of Fracture :**

  If it happened when the part was hot, it's temporary thermal stress.

  If it happened when the part was cool, it's permanent thermal stress.

- **There are only two things that can change :**

  Decrease the tensile stress

  Eliminate or reduce surface defects

- **Understand why glass breaks and manage around it**

Rainbows, Mirages and Talking Over Glass

by
Clifton W. Draper
Lucent Technologies
Bell Laboratories
Princeton, NJ 08542

The simple physics that leads to the refraction and dispersion of sunlight in the lower atmosphere, creating the optical phenomena of rainbows and mirages, is also at the heart of why simple laser light pulses can travel hundreds of miles through glass optical fiber. Bell Laboratories encourages its scientists to speak on technological subjects before wide varieties of audiences. This presentation is a direct result of years of such "Speakers Bureau" type presentations.

Optical fiber is drawn from much larger cylinders of glass known as preforms. These preforms are manufactured around the world using basically one of three processes. These are shown in figure 1. The OVD process was invented and is used by Corning, the

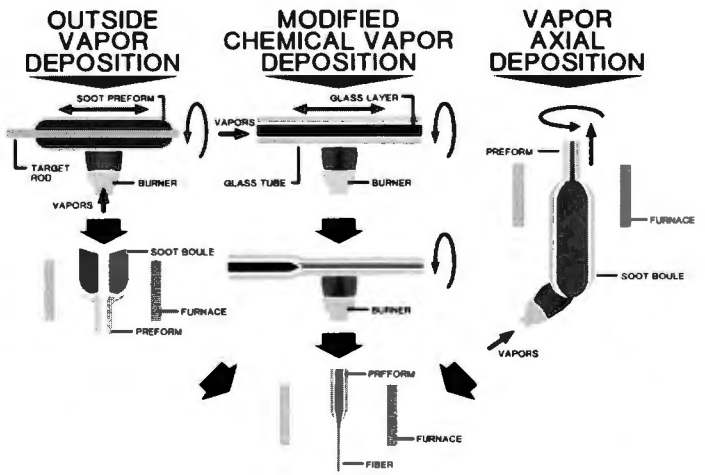

Figure 1

VAD process was developed by Japanese fiber manufacturers, and MCVD was invented at Bell Labs and continues to be the most widely-used manufacturing method. Figure 2 is a schematic of the MCVD process. Basically, a glass-working lathe has a torch that traverses the length of the tube, while vapor-phase chemicals flow down the interior of the silica tube. The index of refraction of the glass is tailored by changing the composition of the various "passes." After deposition is completed, the tube is collapsed into a solid rod. This can be the final preform, or the rod can be overclad with a tube to form a larger glass body. Figure 3 is a schematic of a simple fiber drawing facility. The glass is heated around 2,000 ^{o}C as fiber is pulled from the preform. Laser technology is

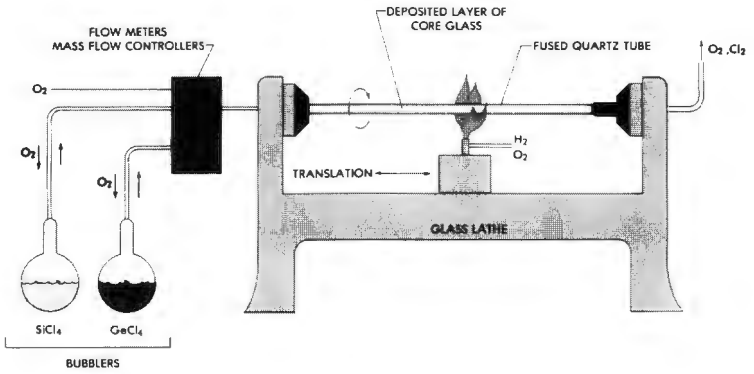

Figure 2

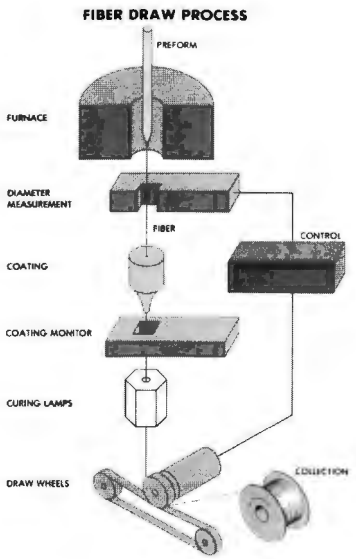

Figure 3

used to control and monitor important fiber parameters like diameter and coating thickness. The glass fiber diameter is 125 micrometers, with a coating od bringing the total diameter to 250 micrometers (see figure 4). Silica optical fiber is inherently very strong, and "tug of war" demonstrations with single strands are a common way to impress on school and lay audiences just how strong glass can be when free of defects. For more information on fiber optics, and demonstrations for school age audiences see reference 1.

Figure 4

Figure 5 is a cross-sectional view of a multimode fiber. The core-to-clad dimensions are exaggerated as typically the graded index profile region has a diameter that is roughly 50% of the fiber diameter. Dispersion (spreading out) of the light pulse is minimized by the graded index profile. Modes traveling the linear path down the center of the fiber, traverse a shorter distance but through material with a higher index of refraction (thus slower propagation velocity). Those following the more torturous path travel a greater distance but on the average through a lower index material (thus faster velocity). At the output end, if the index is designed correctly, the various modes arrive at the same time regardless of path length.

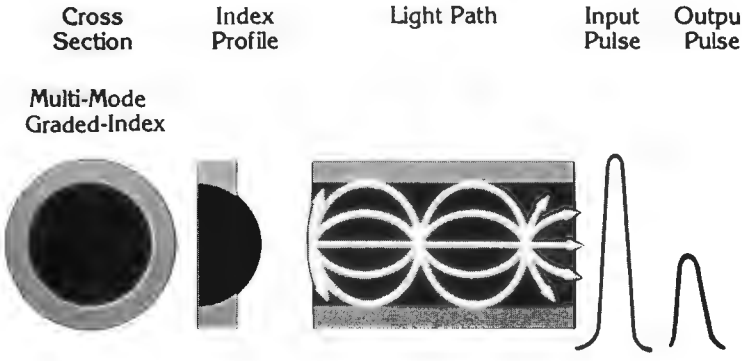

Figure 5

This bending of light (refraction) is the same phenomena that produces the mirages typically found over our roads and highways. Changes in the index of refraction of light in the air are caused by changes in air density, thus air pressure, thus air temperature. Since cold air is more dense, light bends towards (into) cooler air. Figure 6 (courtesy of Robert Greenler[1]) shows a typical inferior mirage, consisting of the images of two motorcyclists and the inverted and "squashed" image of their "reflections" in the caustic (watery looking region). Figure 7 is a schematic drawing with simple ray tracing lines added so one can follow the path of various rays emanating from scattered light off the

Figure 6

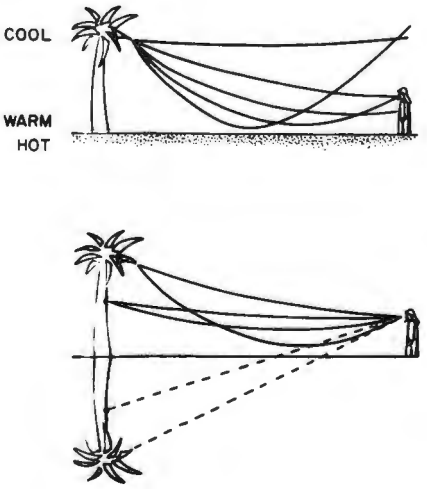

Figure 7

[1] Professor Greenler is also the author of a wonderfully illustrated book. See reference 2.

leaf. Both direct rays (passing through more or less uniform index of refraction air) and rays that have been bent back toward the observer (passing through large temperature gradient) reach our eyes. The result is two images, one upright and "normal" in dimensions, the other "inverted" and often distorted in its physical dimensions. Some fairly strange photographs can be captured if one snaps the picture at the right moment. In figure 8 the roof and rear window of a car are captured just as it goes over a slight crest in the highway. The upright roof, and upright rear window have the *reflected* versions under them, while the entire image is separated from the highway by the inverted image of the sky from above the car.

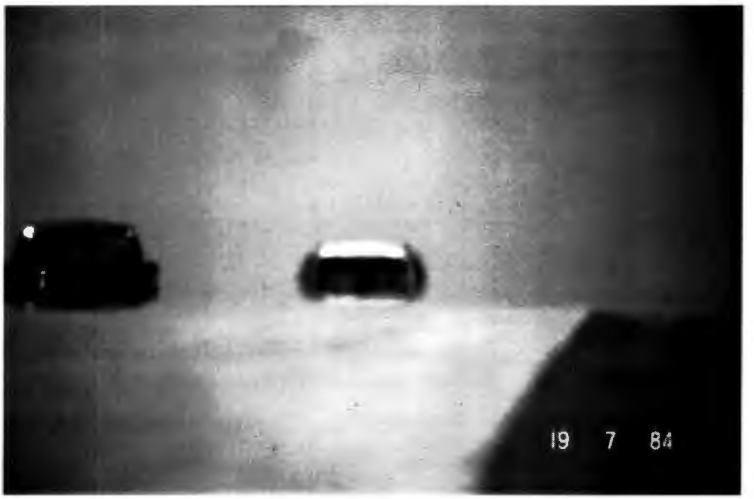

Figure 8

Figure 9 is a schematic that helps to explain how mirages are also found over cold bodies. The air immediately above the water or ice is cooler than the air above it. These are the

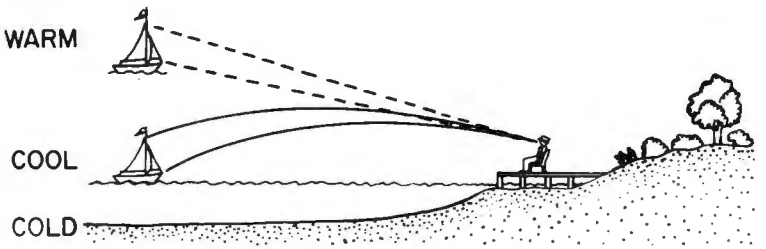

Figure 9

conditions for the superior mirage. Conditions that can produce apparent vertical increases in the dimensions of distant objects. Sailors refer to this as "looming." It is the reason why city lights can often be seen across the Great Lakes, even when light-of-sight and curvature of the earth suggest they cannot. Figure 10 shows grassy shores and beach houses in the distance underneath the Fire Island Bridge on Long Island, NY. Their

Figure 10

vertical features are exaggerated by looming caused as the light traverses over the cool ocean water between the objects and the observer. Superior mirages played an interesting historical footnote in the race for the North Pole at the turn of the 20th century. The Arctic explorers Admiral Peary and Donald MacMillan were both gullible enough to "fall for" the illusion of "Crocker Land." Their respective enthusiasm is well-documented in their logbooks. Figures 11 and 12, again courtesy of Robert Greenler, show how relatively

Figure 11

Figure 12

small pieces of packed ice could indeed appear like a continent of "hills, valleys and snow-capped peaks" waiting to be claimed by the lucky explorer with his dogsled expedition. Of course, since it is just a mirage, when they tramped *inland* over the Arctic Ocean their discovery proved illusive. Figure 13 emphasizes the similarity between lightguiding in a graded index fiber and the superior mirage over a cold surface.

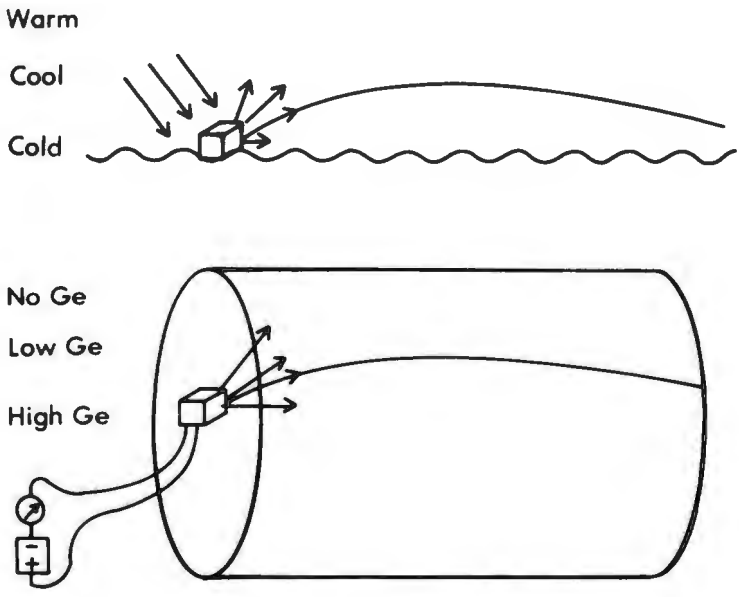

Figure 13

Attenuation and dispersion, illustrated in Figure 14, both present challenges in the quest for infinite bandwidth. Dispersion, the spreading out of different light frequencies

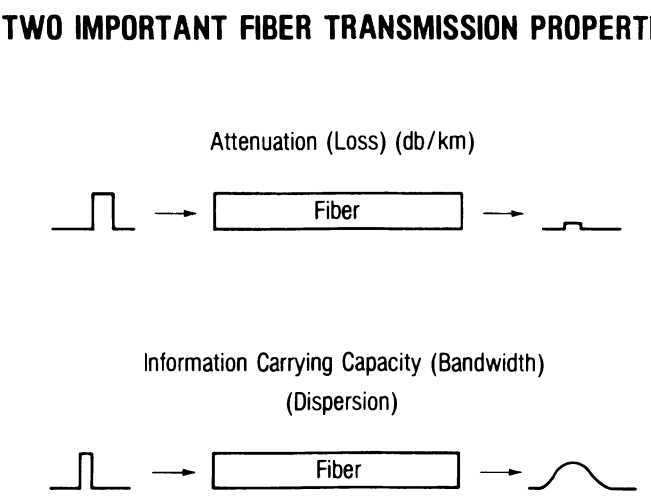

Figure 14

because of slightly different indexes of refraction as a function of wavelength, is what causes the color of the rainbow. Figure 15 illustrates the elements needed for a natural rainbow. Light rays from the sun, raindrops, and an observer. Position yourself with your back to the sun, look at your shadow (anti-solar point) on the ground, and look up at an angle of 42 degrees from your shadow's head. *An extended arm with the hand's pinkie*

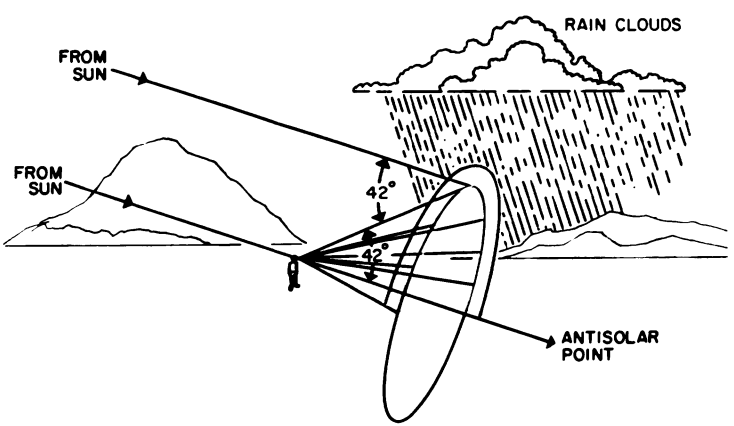

Figure 15

finger and thumb fully stretched apart is about 21 degrees. That is where the primary rainbow will be. The geometry is explained in the schematic of Figure 16. Parallel light

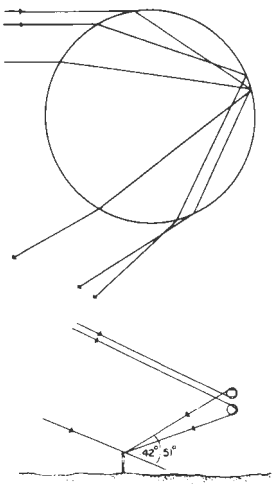

Figure 16

rays from the sun are bent (refracted) along various paths as they enter and exit the raindrop. At certain trajectories light is concentrated. At others it does not exist. Since the index of refraction is slightly different for each wave length of the white light, the colors are dispersed. One or more reflections can occur inside the raindrop. The geometry for the secondary rainbow brings it to the observer at an angle of 50 degrees. Since these light rays had two reflections, the colors are reversed between the primary and secondary bows. That is about all there is to it. Figure 17 summarizes these concepts schematically.

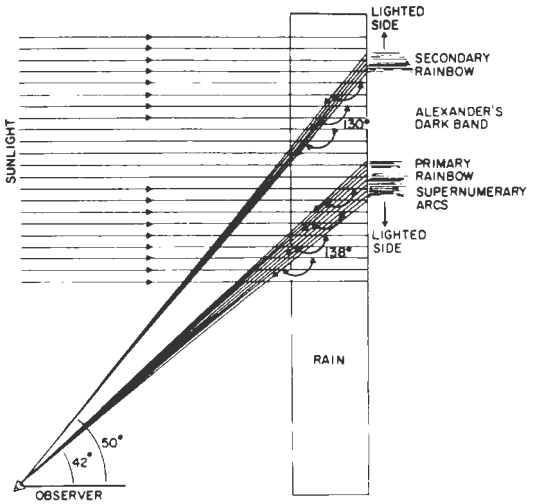

Figure 17

Rainbows can be easily produced with an ordinary garden hose. Figure 18 was made by holding a hose in one hand and a 35 mm camera in the other. The drops were bounced off a two-tone blue VW minibus. Blue is a nice background color. The "sky" is clearly brighter inside the primary bow, and is darker in the region between the bows. Rainbow calendars are very popular for their spectacular bows, as well as because photographic artists have a knack for capturing rainbows with fascinating foregrounds and backgrounds. At least one individual (at the time of this 1999 Glassblowers Society Meeting) was in the business of making spectacular man-made rainbows as part of cultural "events." For more information check out Fred Stern's www.zianet.com/rainbow website.

Figure 18

Figure 19 is a rainbow captured in the Canary Islands. The Canary Islands, Figure 20, were also the site of the first undersea optical cable system trials. TAT 8 was the first optical transatlantic cable and it was put into service in 1988. It turns out that the optical cable installed in the Canary Islands was suffering from "shark attacks." A telecommunications hazard first! Since this was the first optical system, a great deal was *riding on it*, and AT&T was particularly concerned about this unexpected finding. It was a well-kept "nondisclosure," and quite a few engineers and managers lost sleep over it. Bell Labs engineers are not totally without a sense of humor though, and one popular cartoon amongst the "insiders" showed a shark at the dinner table with a strand of cable across his plate, knife and fork in fin. The cartoon caption read "AT&T the right choice," the company advertising slogan at the time. In the end it turned out that the shark bites were simply the result of inadvertently placing the cable in a shark feeding area. It had nothing to do with ion currents in the water around the cable, and a yet-to-be-discovered shark internal conductance meter.

Figure 19

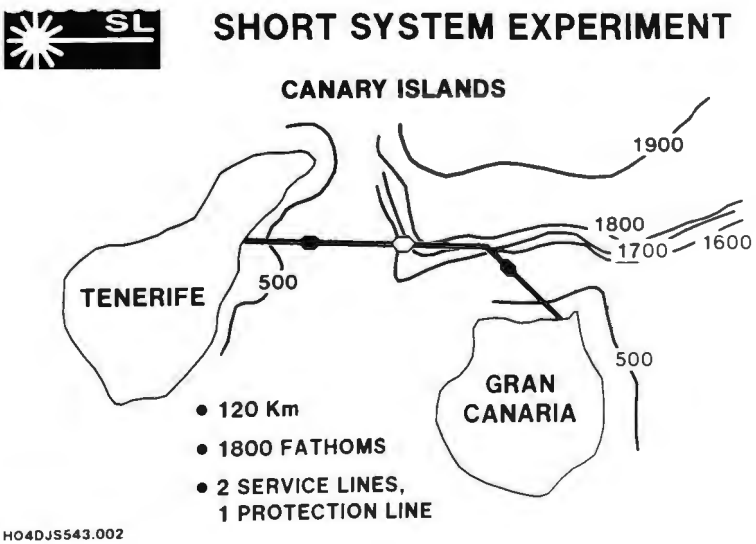

Figure 20

Figure 21 shows a lightning strike density map of the continental United States. Lightning strikes, as well the reader can imagine, represent a real telecommunications hazard. Figure 22 shows a density map for another hazard to telecommunications. This is typically the final slide in my presentation, and the person in the audience that can, in Jeopardy question form, correctly question the answer wins a twenty dollar bill. It took quite a few ASGS members and meeting attendees to get to the correct answer, but it was finally found. If you have read this far, and you really want to find "What hazard to telecommunications is depicted in Figure 22," then email me at cwdraper@lucent.com or alternatively ask a fellow glassblower who happened to be in attendance.

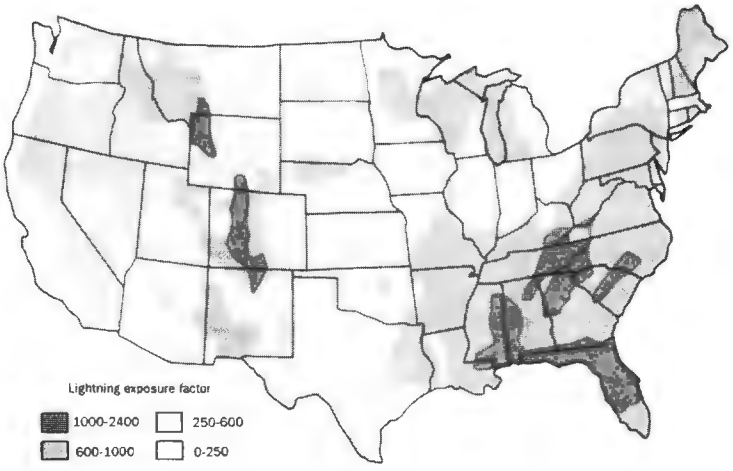

Figure 21

Figure 22

References

1. C.W. Draper, "Talking Over Glass: Learning Transmission Rates Through the Telephone Game," *MRS Bulletin* (November, 1992): pp. 93-95.
2. R. Greenler, Rainbows, Halos, and Glories (London: Cambridge University. Press, 1980). Reprinted in paperback, 1999, by Peanut Butter Publishing and available through Blue Sky Associates (tel. 414-377-1498).

The Technique of Silver Soldering Various Metals to Glass for Laboratory Applications

by
Edwin A. Powell
AstraZeneca, Inc.
Wilmington, Delaware 19850-5437

The scientific glassblower has often searched for a method of easily sealing metal to glass. This method allows the glassblower the ability to seal various metals to glass with very little difficulty and heat. The sealing process involves the use of silver solder and a silver matrix.

It is important to select the proper solder. The solder in question had to be as inert as possible and needed to have a low melting point to eliminate the possibility of causing strain to develop in the glass. A silver solder that was 96% tin and 4% silver and had a melting point of 221° C was chosen. This solder is stronger than the traditional tin/lead solder and eliminates lead found in the more common solders. This solder is also compatible with a wide range of metals. The 96% tin and 4% silver solder has a high surface tension which allows it to fill gaps between the glass and the metal. A clear flux recommended by the manufacturer was used.

Several heating methods, from the traditional soldering iron to a high temperature heat gun as shown in Fig.1, were used to achieve the desired results. The soldering iron selected was a 370°C iron with a controlled tip. A controlled tip iron maintains its temperature during the soldering process and eliminates the loss of heat through heat sinking.

Figure 1. High Temperature Heat Gun and Soldering Iron

The selected heat gun has a variable temperature setting. It produces 1740 watts with a maximum temperature of 540° C. The variable heat setting provides the ability to match the temperature to the size of the pieces to be soldered. A 1/4" pinpoint nozzle attachment directed the hot air to a specific area. Two heat guns with small nozzles were used to concentrate the heat. The nozzles need to be as close as possible to the pieces being soldered, since heat will be lost as the hot air is dispersed. The use of hot air and the low temperature solder eliminates oxidation of the pieces that are soldered, stainless steel thus remains bright and free from oxidation.

A silver matrix or decal (Fig.2) is used to provide a soldering bridge from the metal to the glass. The decal which is applied to the glass is a vitrifiable silver pigment on specially coated paper and topped with a cover coat to hold the silver together once immersed in water. The decals can be manufactured in many different configurations, such as round or rectangular, so selection of an appropriate size and shape for the situation is recommended. The decal is applied by first wetting the decal and sliding the silver portion off the paper backing; the decal is then positioned over the hole. It is important that the decal lie flat on the glass. The decals may be removed by aqua regia (three parts concentrated HCl and one part of concentrated HNO_3).

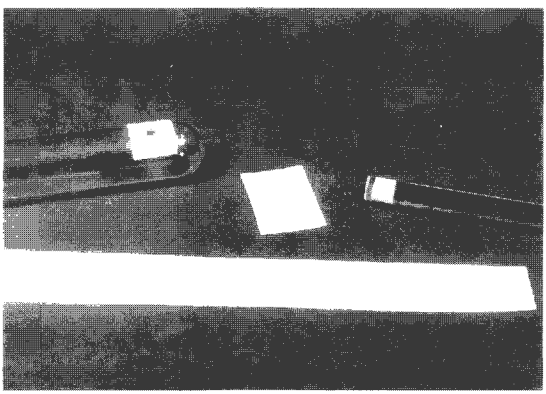

Figure 2. Silver Decal

Soldering the various metals to the glass starts with the preparation of the hole. A hole is opened in the glass tubing either by blowing the hole out or by drilling. The hole must be flush with the outside surface of the tube or flat surface. The hole should be a tight fit between the wire and the glass tubing. This preparation of the hole for wire soldering is critical. The silver decal is applied and placed in an annealing oven; the annealing oven is brought to 565° C and then cooled. The wire is then inserted in the hole and held in place by a fixture. A small amount of flux is applied to both the wire and the silver decaled glass. The soldering iron (Fig.3) is applied to the wire. The iron is then moved down the wire and the solder is introduced to both parts to complete the joint. Since solders tend to flow toward the source of heat, position the pieces to be soldered so as to allow the solder to flow down the wire. This will permit the solder to cover the joint completely. Since glass is a poor conductor of heat, the solder will not readily flow to

the cool surface of the glass. The procedure for wire (Fig.4) or small metal tubing (Fig.5) is the same.

Figure 3. Soldering Wire

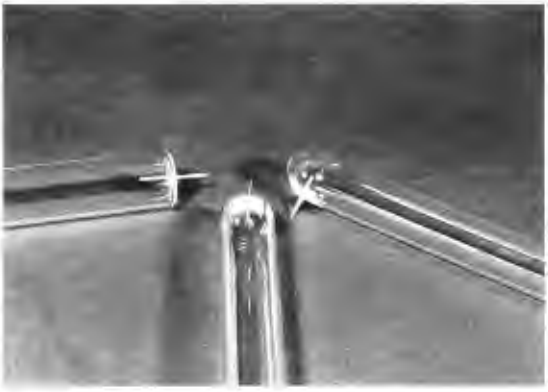

Figure 4. Wire Soldering

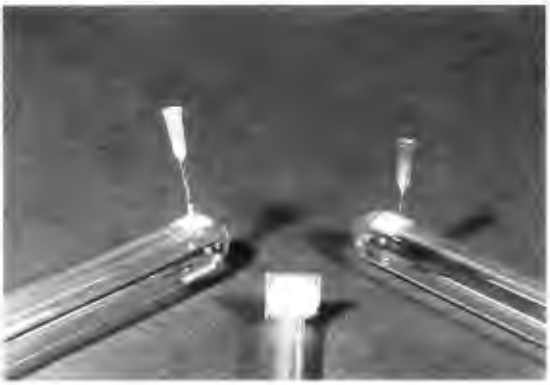

Figure 5. Soldering Tubes and Flat Stainless Steel

Soldering wire and flat surfaces to glass, under continuous pumping, produced vacuum results in the range of 20 to 40 millitorr. A stainless steel flat soldered to a modified o-ring joint (similar to a 12/5 ball joint) achieved a vacuum of 20 millitorr. Platinum wire, 0.020" in diameter soldered through the side of a 22mm od borosilicate tube achieved a vacuum of 35 millitorr.

A heat gun is used for joining a glass tube to metal tubing (Fig.6) end to end. In this situation, the decal is applied around the end of the glass tube. The metal tube is first tinned or coated with a thin layer of solder on the inside. Excess solder is removed to allow a tight fit with the glass. The glass tube and the metal tube are held in a glassblowing lathe. Flux is applied and the two tubes are brought together. The glass tube is inserted into the metal tube and the two are positioned with a small strip of the silver decal visible. Using two heat guns affixed with 1/4" nozzles as shown in Fig.7, heat is applied from both sides as the glass tube and the metal tube are slowly rotated in the lathe. The time it takes to complete the joint depends on the size and thickness of the metal tube. It is preferable to use a thin tube to allow good heat transfer. The thickness of the metal is determined by structural requirements.

Figure 6. Soldering Tubing

Figure 7. Lathe Soldering

The use of small o-ring joints work very well for soldering to flat metal surfaces. First, the o-ring groove is removed by grinding. The decal is then applied to the flat surface of the glass and annealed. After annealing, the flat metal piece is tinned with the 96% tin and 4% silver solder. The flux is then applied and the tinned metal is placed on the decaled surface. The heat gun is used, applying the heat only to the metal surface.

A traditional gas/oxygen hand torch can be used, but care must be taken to avoid overheating. A very soft flame is used, but inducing strain in the glass is a problem. With the torch it is difficult to concentrate the heat in a specific area. The traditional hand torch produces too much heat and should be avoided. The preference is a soldering iron or heat gun.

Overheating the flux will cause soldering problems. If the flux turns black, it has been destroyed and soldering cannot be accomplished. At this time it is necessary to remove all of the black residue and clean the metal to a bright surface. Overheating with a soldering iron or high temperature heat gun can induce strain in glasses. Prolonged heating and excessive heat at high temperatures must be avoided.

Advantages

Low heat sealing
No special equipment
The ability to seal a variety of metals in a small area
Stainless steel quickly soldered to glass
Complicated glassware can be fabricated first and then the metal can be sealed in using minimal heat
Achieve low vacuum
Insulated wire can be attached inside a tube after annealing.

Disadvantages

Introduction of additional metals, the solder
Residual flux must be removed
Wire and tubes not high vacuum
Does not tolerate high temperatures

Conclusion

All glasses that have reasonable thermal properties will allow the glassblower the ability to solder to those glasses. Borosilicate and quartz glass is the most desirable for this technique. It is conceivable that any specialty glass with a reasonable thermal property can be soldered to a metal. This technique should be considered an alternative for traditional glass to metal sealing.

Acknowledgments

CCES Co., PO Box 673, Hatboro, PA 19040
Silver Decals
J.W. Harris Co., Inc., 10930 Deerfield Road, Cincinnati, OH 45242
Stay-Brite Silver-Bearing Solder
Stay-Clean Flux
Master Appliance, 2420 18th Street, Racine, WI 53401
Varitemp Heat Gun Model VT-750C
1/4" Pinpoint Attachment no.51309
Weller Soldering Iron
Power unit TC-202
Iron TC-201-P

Technical Posters 1999

Waine Archer – "Technical Writing for Non-Writers"
Los Alamos National Lab
P.O. Box 1663 M/SD 478
Los Alamos, NM 87544
(505) 667-4867
marcher@lanl.gov

Joseph Gregar – "Construction of the Gregar Extractor"
Argonne National Laboratory
9700 South Cass Avenue
Argonne, IL 60439
(630) 252-3550
jgregar@anl.gov

Gary Gregston – "A Constant Temperature Gas Mixing Humidifier"
Lockhead Martin Idaho Tech Company
P.O. Box 1625
Idaho Falls, ID 83415
(208) 526-3470
ggregsto@inel.gov

Doni Hatz – "Custom Sizes of Square and Rectangular Tubing"
Procter and Gamble Company
Miami Valley Labs
P.O. Box 538707
Loveland, OH 45140
(513) 627-2313
hatzdj@pg.com

James Hodgson – "Math for Glassblowers"
Kansas State University
Department of Chemistry
111 Willard Hall
Manhattan, KS 66506
(785) 532-6676
Hodgson@ksu.edu

Georges Kopp – "A Versatile Modified Chuck for the Lathe"
McGill University
Otto Mass Chemistry Building
801 Sherbrooke West
Montreal, Quebec H3A 2K6
Canada
(514) 398-6217
Kopp@chemistry.mcgill.ca

Sharon Skenandore – "The Forming of Specific Volume, Shaped, Threaded Glass Bottles"
Bechtel Bwxt Idaho
PO Box 1625
Idaho Falls, ID 83415
(208) 526-8362
sns@inel.gov

David Wedsworth – "A Custom Glass Box"
Eli Lilly & Company
Lilly Corp. Center
Mail drop 0502
Indianapolis, IN 46285
(317) 276-4107
dswedsworth@Lilly.com

Technical Workshops 1999

Dennis Briening - *Hercules Research*
"Blow-molding Thin Walled Thermal Analysis Cells"

Allan Brown - *University of Connecticut*
"Devitrification of Borosilicate Glasses; What Causes it? How can we reverse it?"

Richard Gerhart - *California Institute of Tech*
"Making Quartz Ring Flanges by Laminating"

David Goldstein - *Precision Glasswork, Inc.*
"Low Expansion Color Borosilicate Glass"

Joseph Gregar - *Argonne National Labs*
"The Triple Seal for the Gregar Extractor"

Mike Greico - *V.M. Glass Co.*
"Tooling Threads onto Borosilicate Glass"

Barry Lafler - *Brookhaven National Lab*
"Air Free Sampling Cell"

Wayne Martin - *M & M Glassblowing, Inc.*
"Graded Seals: Borosilicate to Quartz"

Bill Roach - *Wale Apparatus*
"Litton Lathe Upgrades and Repair"

Mike Souza - *Princeton University*
"Fabricating No-blow Multi-necked Flasks"

Mike Souza - *Princeton University*
"Flame-working G.E. 180 Aluminosilicate Glass"

Karl Walther - *KAWAL Research Glass*
"Pt Sealing to Borosilicate Glass"

The video versions of these Technical Workshops are in the ASGS video library and are available to be loaned out.

1999 Exhibitors

Andrews Glass Co.
3740 N. West Blvd.
Vineland, NJ 08360
Tel: (609) 692-4435
Fax: (609) 692-5357
mail@andrews-glass.com

Aura Lens Products
Box 763
St. Cloud, MN 56302-0763
Tel: (320) 253-0919
(800) 281-0287
Fax: (320) 253-1239
mike@auralens.com

B&C Glastechnische; Maschinenbau und Vertriebs-GmbH
Lahnwegsberg5-7
D-35435 Wettenberg (Launsbach)
Germany
Tel: 641-82009
Fax: 641-84204

Blue Flame Technology
431 Kentucky Lane
McKinney, Texas 75069
Tel: (972) 542-2571
Fax: (972) 562-9896
bflamel@airmail.net

Carlisle Machine Works
P.O. Box 746
Millville, NJ 08332
Tel: (609) 825-0627
Fax: (609) 825-5510
carlisle@cybernet.net

Chemglass Inc.
3861 N. Mill Road
Vineland, NJ 08360
Tel: (800) 843-1794
Fax: (800) 922-4361
Steve@chemglass.com

Corning Incorporated
Marketing Services, BF-02
Corning, NY 14831
Tel: (607) 974-0388
Fax: (607) 974-0292
clinejn@corning.com

Dynacut Inc.
3425 Funk Mill Rd.
P.O. Box 156
Springtown, PA 18081
Tel: (610) 346-7386
Fax: (610) 346-6770
rplatt@itw.com

EVAC Int.
215 River Vale
River Vale, NJ 07675
Tel: (201) 666-8558
Fax: (201) 666-8470
evac@bigfoot.com

Friedrich & Dimmock
P.O. Box 230
2127 Wheaton Ave.
Millville, NJ 08332
Tel: (609) 825-0305
Fax: (609) 327-4299

Glass Tech. Supplies
1128 East Valencia Dr.
Fullerton, CA 92831
Tel: (714) 630-0483
Fax: (714) 630-1176
valulab@yahoo.com

Glass Torch Tech. Inc.
1988 Herbert Ave.
Hellertown, PA 18055-1739
Tel: (610) 838-2446

Glass Warehouse
P.O. Box 1039
1501 N. 10th Street
Millville, NJ 08332
Tel: (800) 833-0410
Fax: (609) 825-9014
glass.warehouse@wheaton.com

G.M. Associates Inc/ Herbert Arnold
9824 Kitty Lane
Oakland, CA 94603
Tel: (510) 430-0806
Fax: (510) 562-9809
deboran@gmassoc.com

Heathway Inc.
1620 Cross Creek Court
Bethlehem, PA 18901
Tel: (215) 348-2881
Fax: (215) 348-2309
heathway-usa@compuserve.com

Heritage Insurance Agency Inc.
1317 South Main Rd.
Professional Center
Vineland, NJ 08360
Tel: (609) 696-3152
Fax: (609) 696-0115

Kimble/Kontes
1022 Spruce Street
Vineland, NJ 08360
Tel: (609) 962-8500
Fax: (609) 962-8134
kimkon@acy.digex.net

Larson Electronic Glass
P.O. Box 371
2840 Bay Road
Redwood City, CA 94064
Tel: (650) 369-6734
Fax: (650) 369-0728
gls2mtl@juno.com

Litton Eng. Lab.
200 Litton Dr., Suite 200
Grass Valley, CA 95945
Tel: (530) 273-6176
Fax: (530) 477-1068
gkoopman@littonengr.com

Macalaster Bicknell Co. of NJ Inc.
P.O. Box 109,
North & Depot Sts.
Millville, NJ 08332-0109
Tel: (609) 825-3222
Fax: (609) 825-3375
macbicknj@cybernet.net

M-Tech Industries
P.O. Box 1358
Cedar Ridge, CA 95924
Tel: (530) 269-2137
Fax: (530) 269-2930
vwmmtind@aol.com

Nortel Machinery Inc.
1051 Clinton Street
Buffalo, NY 14206
Tel: (716) 852-2685
Fax: (716) 825-6374

North Jersey Diamond Wheel
218 Little Fall Road
Cedar Grove, NJ 07009
Tel: (973) 239-5808
Fax: (973) 239-6288
bonnie@diamondwheels.com

Pedco-Hill
P.O. Box 89
Ambler, PA 19002
Tel: (215) 646-7974
Fax: (215) 646-6875
pedcohill@erols.com

Pegasus Industrial Specialties Inc.
530 Massey Rd.
Guelph, ONT N1K 1B4 CANADA
Tel: (800) 315-0387
Fax: (519) 766-1492
rtrent@pegasus-glass.com

Preston Glass Company Inc.
P.O. Box 475
Glen Oaks, NY 11004
Tel: (718) 596-8641
Fax: (718) 596-8646
preston_glass@msn.com

Quartz Products/Saint-Gobain
1600 West Lee Street
Louisville, KY 40201-7409
Tel: (502) 775-7367
Fax: (502) 775-7354
daryl.terry@sgcna.com

R&H Filter Co. Inc.
3 Baltimore Ave.
Georgetown, DE 19947
Tel: (800) 553-6294
Fax: (302) 856-1503
glassfilter@ce.net

Schott Corporation
3 Odell Plaza
Yonkers, NY 10701-1405
Tel: (914) 378-3861
Fax: (914) 968-8585
blackwell@schottglass.com

SMS Technologies Inc.
3531 Everingin Road
Monroeville, OH 44847
Tel: (419) 465-4175
Fax: (419) 465-2873
smstechnologies @nwonline.net

Tecnolux Inc.
103 14th Street
Brooklyn, NY 11215
Tel: (718) 369-3900
Fax: (718) 369-2845
info@TecnoLux.com

V.M. Glass Co.
3231 N. Mill Road
Vineland, NJ 08360
Tel: (800) 400-6625
Fax: (609) 794-9695
airvair@aol.com

Wale Apparatus Co., Inc.
400 Front Street
Hellertown, PA 18055
Tel: (610) 838-7047
Fax: (610) 838-7440
waleapp@aol.com

Wilmad/Labglass
P.O. Box 688
1002 Harding Hwy.
Buena, NJ 08310
TelTel: (609) 697-3000
Fax: (609) 697-0536
mkt@wilmad.com

Wilt Industries Inc.
Rt. 8
Lake Pleasant, NY 12108
Tel: (800) 232-9458
Fax: (518) 548-5504
wilt@klinknet.com

44th Symposium Attendees

Jim Abbott
David Ablon
Lisa Allen
Pat Allen
Francisco Alvarez
Jose Alvarez Chavez
Jeffery Anderson
Mark Anthony
Arthur Arias
Michael Arias
Robert Aurelius
J. Jeffrey Babbitt
Ruth Babbitt
Tom Baker
Ron Barnes
Karen Barsuglia
Lori Bartley
Ron Belciano
Emmanuel Bellantoni
Robert Benard
Albert Bensimon
Ronald Bihler
Bryan Bivins
Dave Black
Pat Blake
Richard Bock
Günther Boepple
Henry Boerner III
Walter Boger
Theodore Bolan
Anastacio Bonilla
Frank Bosco
William Bourbeau
Ken Brick
Dennis Briening
Allan Brown
Marylin Brown
Holly Brucker
James Byrnes
William Caldwell
Chris Camac
Deborah Camp
Glen Campbell
John Caparelli
Karen Carraro
Max Carraro
Royce Carter
Joe Caruso
Dr. Gordon Cates
John Chabot
Shirley Charlton
Domenic Ciancarelli
Francis Ciancarelli
Larry Circosta
Bonnie Clark
Jo Clark
Wendall Clark
Brenda Cloninger
Jerry Cloninger
Tim Condas
Bob Connoly
Murray Connors
Jack Conrad
James Cornell
LuAnn Cossaboon
Dumitru Costea
Dennis Courtney
Andy Coyne
Gary Coyne
Mara Coyne
Stacy Coyne
Chip Crider
Michael Curcio
William Curtis
Renate D'Angelo
Dave Daenzer
Katrina Daenzer
Sean Daenzer
Patrick Deflorio
Ralph DelBuono
Barb DeMasi
Cindy Dichino
Richard Dickinson
Brian Ditchburn
Darcey Doering
Elaine Doering
Arthur Dolenga
Carol Dolenga
Mary Dolenga
Frank Dougherty
James Downey
Wayne Downs
Dr. Katie Carrado-Gregar
Dr. Clifton Draper
Timothy Drier
Tracy Drier
Alan Durham
Thomas Dusek
Ruth Dykstra
Daniel Edwards
Diane Edwards
Lisa Edwards
Mark Engler
Robert Evans
Kenneth Everingham
Gary Farlow
Marcus Fend
Hans Florell
Maryann Florell
Robert Forgnoni
John French
Pamela Geddes
Richard Gerhart
Hans Geyer
Robert Goffredi
David Goldstein
Bruce Golway
Robert Greer
Ruth Greer
Joseph Gregar
Gary Gregston
Michael Greico
Adolf Gunther
Inge Gunther
Nancy Hagmaien
Robert Halbreiner
Richard Harrison
Terri Hartman
Bruce Harwood
Doni Hatz
Ann Haymaker
Howard Hayman
Frank Hedges
Timothy Henthorne
Hiroko Herbert
Volker Herbert
Thomas Herr
Scott Hiemstra
Newton Hill
Darlene Hoare
Dawn Hodgkins
Donald Hodgkins
James Hodgson
Jan Holbert
Willy Horn
Connie House
Thomas Howe
Tollie Howe
Michelle Johnson
William Jones
Nick Jozanovie
Linda Kellc
Nontas Kontes
Gary Koopman
Georges Kopp
Timothy Kornahrens
Charles Kraft
Gary Krevitski
Fridolin Kummer
Hedi Kummer
Peter L'abbe
Barry Lafler

Tim Lamparello
Elke Langer
Manfed Langer
JoAnn Lathbury
Patrick Lathbury
Rand LeBaron
Steve Leek
Robert LeFrancois
Helen Legge
John Legge
Philip Legge
Ronald Legge
Sherri Legge
L. Frederick Leslie
Meryl Leslie
Robert Lewandowski
Eliot Lightner
Donald Lillie
Maxine Lillie
Charles Litton, Jr.
Dave Lobley
William Logsdon
Dave London
Valerie London
J. Peter Lunzer
Roswitha Lutz
Glenn Malone
Wayne Martin
Wilbur Mateyka
Victor Mathews
Robert McAnally
Darren McGinnis
Bill McLaughlin
Frank Meints
James Merritt
Craig Millron
Elnora Mills
Hedy Misch
Manfred Misch
Steven Dean Moder
Marvin Molodow
Michael Morris
David Mortimer
Emile Munschy
Thomas Murphy
Craig Nagami
T. Thomas Nagami
Anthony Gene Nelson
Robert Nichols
Peter Norton
Jeff Noyes
Mary O'Brien
Dan O'Grady
Gawain Ortiz
Kenneth Owens
Bob Pacik
Joe Paciulla
Malcolm Pack
Michael Palleschi
Michael Palme
Angie Parillo
Edward Parillo
Joseph Partlow
Mary Partlow
Jack Partridge
Vikram Patel
Gary Pedersen
Victor Pesce
Amy Phillips
Dorothy Platt
Robert Platt II
Joe Plumbo
John Plumbo
Anthony Pomponio
Robert Ponton
Edwin Powell
Sally Prasch
Daniel Preston
Padma Ramalingham
Louis Rivera
Bill Roach
Edwin Rodda
Hans Rohner
David Roman
Michael Ronalter
Harold Russo
Steve Russo
Ottmar Safferling
Megumi Sager
Steven Sager
William Sales
Eugene Sasville
Kevin Scanlin
Maria Schlott
Rudolf Schlott
Gayle Schlueter
Josef Schmitz
Stan Schug
Christine Schul
Hope Schul
Thomas Schul
Brian Schwandt
A Ben Seal
Joan Seal
Randolph Searle
Nettie Severn
Peter Severn
William Sexton
Herbert Sherente
Terry Shidner
Robert Singer
Jan Singhass
Ron Sjolander
Sharon Skenandore
Sue Slater
Gail Slegel
Russell Slegel
David Smart
Daryl Smith
Bradley Smith
Lorraine Smith
Richard Smith
Dianne Socha
John Socoloski
Jeff Sorgler
Mary Souza
Michael Souza
Scott Sowders
Joan Speakman
William Spencer
Christopher Sprague
Jayne Sprague
Bruce Staats
Thomas Stefanek
Dennis Steffey
Jeremy Stoneback
Parker Stowman
David Surdam
Phil Surdam
Walt Surdam
Robert Sweeney
Debbie Taylor
Ralph Taylor
John "Mike" Trembly
Kathy Trent
Ron Trent
Tom Unger
Lisa Vanegas
Daniel Vogt
W.P. Wagelaar
Pei Wai
Gene Wakeley
Joseph Walas
Robert Wallace
Karl Walther
Steven Ware
Andrew Wargo
Tami Wargo
David Wedsworth
Jerry Weido
Peter Weier
Peter Werner
Lanah Wheeler
Michael Wheeler
Mark Wicker
Randolph Wilkin
Daniel Wilt
William Wilt
Donald Woodyard
Craig Wurzel
Heather Young
Jody Young
Jay Zahran